Analysis of Drift Errors in the JPL/UCLA Micromachined Gyroscope

by

Indrani Chakraborty

Submitted to the Department of Mechanical Engineering
in partial fulfillment of the requirements for the degrees of

Bachelor of Science

and

Master of Science

at the

MASSACHUSETTS INSTITUTE OF TECHNOLOGY

May 1996

Author . . . .
Department of Mechanical Engineering
May 10, 1996

Certified by. . . . .
Alexander Slocum
Professor of Mechanical Engineering, MIT
Thesis Supervisor

Accept . . . .
A in A. Sonin
Chairman, Departmental Committee on Graduate Students

Analysis of Drift Errors in the JPL/UCLA Micromachined Gyroscope

by

Indrani Chakraborty

Submitted to t he 1 Department of Mechanical Engineering
on May 1o, 1996, in partial fulfillment of the
requirements for t he degrees of
Bachelor of Science
and
Mast er of Science

Abstract

The model of the JPL/UCLA micromachined vibratory gyroscope will be enhanced to include time varying effects. First, they will be shown to exist through trends in the experimental results. Causes of mechanical error will be further explained by analyzing possible perturbations to the physical model. Then, a method will be presented to develop a computer simulation of any specific gyroscope, based on empirical data, which will approach the actual behavior more closely than do the current theoretical equations. Finally, recommendations will be made for removing some of the drift error, thereby improving the gyroscope performance.

Thesis Supervisor: Alexander Slocum
Title: Professor of Mechanical Engineering, MIT

Analysis of Drift Errors in the JPL/UCLA Micromachined Gyroscope

Gyroscope

by

Indrani Chakraborty

Abstract

The model of the JPL/UCLA micromachined vibratory gyroscope will be enhanced to include time varying effects. First, they will be shown to exist through trends in the experimental results. Causes of mechanical error will be further explained by analyzing possible perturbations to the physical model. Then, a method will be presented to develop a computer simulation of any specific gyroscope, based on empirical data, which will approach the actual behavior more closely than do the current theoretical equations. Finally, recommendations will be made for removing some of the drift error, thereby improving the gyroscope performance.

Thesis Supervisor: Alexander Slocum
Title: Professor of Mechanical Engineering, MIT

Acknowledgments

Contents

List of Figures

List of Tables

Chapter 1

Introduction

Recently, NASA has adopt ed a mission to develop "smaller, faster, cheaper, and better" spacecraft. The idea is to launch several low cost missions in the place O f one massive space probe. One of the pivotal challenges to this new philosophy is to develop "lighter" scientific payloads, or smaller, low mass, low power, and low cost instrumentation. The science of microelec tromecha nical systems (MEMS), which uses micromachining technology developed by the semiconductor industry to build micromechanical structures, is perfectly positioned to meet these goals.

Among the instruments M EMS researchers are striving to perfect, the g yroscope is receiving considerable att ention. Most of the work being done is in the area of vibratory gyroscopes, which have no moving parts and require less power than tra-ditional rotational schemes. The idea is that if a mass is moving along a straight line trajectory and an angular rate i s applied perpendicular to this linear motion, the Coriolis force will push the mass in the third perpedicular axis, as shown in fig-ure 1-1a. Therefore, if a mass is made to vibrate along the instrument x axis, an applied angular rate in the z direction will cause a vibration along the y axis that is a surpressed carrier frequency representation of the ang ular rat e, as shown in figure 1-1 b. This effect allows perfect decoupling of drive and sense, and is theoretically an excellent method of gyroscopic detection.

In the past, vibratory gyroscopes have been largely impractical. The man hours required to machine a mass which w ould travel t he drive tra jectory perfectly were
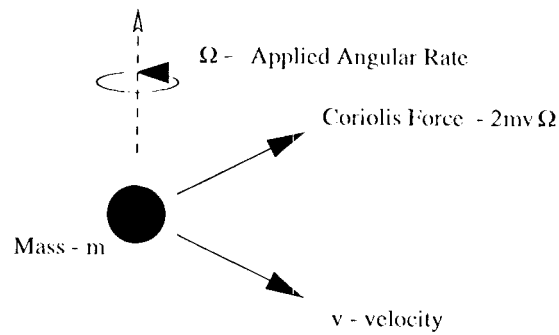
a) Coliolis Force on a Moving Mass
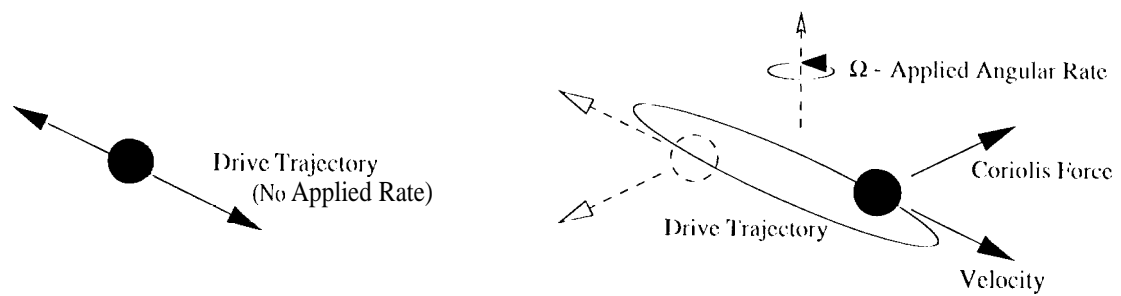
b) Vibratory Drive Paths and Coriolis Force

Figure 1-1: Coriolis Forces Acting on Moving Masses

too expensive to compete with rotational gyroscopes. However, perfect machining is a far more attainable goal in M EMS. Unfortunately, in general MEMS gyroscopes developed to date are so low mass that they do not have the resolution to compete with entrenched larger gyros, even for space applications. The JPL/UCLA gyro is heavier than most. Unfortunately, it suffers from man y of the machining problems of its ancestors, since currently the vibrati ng mass is not micro machined. These random, time varying problems need to be incorporated into a simple model which can then be used to sim ulate actual gyro response as well as to develop robust driving and sensing schemes and optimize performance.

Chapter 2 describes the JPL/UCLA microgyroscope, and the current physical model. Chapter **3** outlines the testing process **for** prototype **gyros**, examines the results, and lists deficiencies in the theotetical model. These are then corrected in chatper **4** by examining small perturbations and stochastic effects. In chapter 5, the test data is used to put magnitudes on the new model, a n d the computer program used to simulate the gyroscope i s presented. Chapter 6 suggests improvements to eliminate some drift error. Conclusions are summarized in chapter 7.

Chapter 2

JPL/UCLA Micromachined Vibratory Gyroscope

2.1 Operation

The JPL/UCLA gyroscope is depicted in figure 2-1. It is also known as the "cloverleaf" gyroscope. The outer frame, support cantilevers, and paddles are etched as one piece from a single crystal silicon (SCS) wafer. The post, on the other hand, is macromachined separately from brass, manually inserted into a hole at the center of the paddles and glued in place. This assembly is then mounted onto a quartz baseplate, which has four metal electrodes that line up under the four paddles.

Mechanically, the post and cloverleaf structure form a second order system where the post is the mass and the cantilevers are the springs. From the support geometry, it is assumed that the mass undergoes negligible translational displacements in the instrument frame, and therefore only rotational displacements need to be discussed. Figure 2-1 shows the three possible rotational displacements, and the three corresponding fundamental vibrational node lines. In open air, the system is extremely overdamped. Under vacuum, all these modes become resonant.

The entire cloverleaf assembly is electrically grounded. However, the metal electrodes on the baseplate are not. Therefore, when voltages are applied to the baseplate, an electrostatic force is created which can move both the cloverleaf and the post. ¶¶¶

Axis	$I\left(gm \cdot cm^2\right)$	$\kappa\left(\frac{dyn}{cm}\right)$	$\alpha\left(\frac{dyn \cdot cm}{rad/sec}\right)$
θ	10^{-4}	10^3	10^{-4}
ψ	10^{-4}	10^3	10^{-4}
ϕ	10^{-5}	10^3	10^{-4}

Table 2.1: Typical Values for Physical Parameters

particular, applying a voltage under M1 and M2 causes movement around the θ or drive axis. The gyroscope is driven by applying a strictly positive periodic waveform to these paddles at the resonant frequency of the θ mode.

The application of a coriolis force to the instrument z axis will cause the post to precess. This motion can be detected and measured by monitoring the difference in the displacements of paddles M3 and M4. For small movements, the current caused by a change in capacitance between the paddle and the baseplate is almost linearly proportional to the time rate of change of the displacement. Therefore, a circuit capable of sensing the current generated by each of the two paddle-electrode pairs and then subtracting them will actually be producing a voltage representation of the velocity of vibration along the ψ or sense axis. The amplitude of this waveform is proportional to the angular rate. Note also that by adding the two signals, one can also produce a representation of the velocity of the vibrations along the drive axis.

2.2 Theoretical Model

2.2.1 System

As stated above, the structure acts like a second order mass-spring-damper system. Therefore, for the three degrees of rotational freedom, one may begin with the following general equations:

$$I_\theta \ddot{\theta} + \alpha_\theta \dot{\theta} + \kappa_\theta \theta = Torque_\theta(V_{in}, \Omega_x, \Omega_y, \Omega_z, \theta, \psi, \phi) \qquad (2.1)$$

13
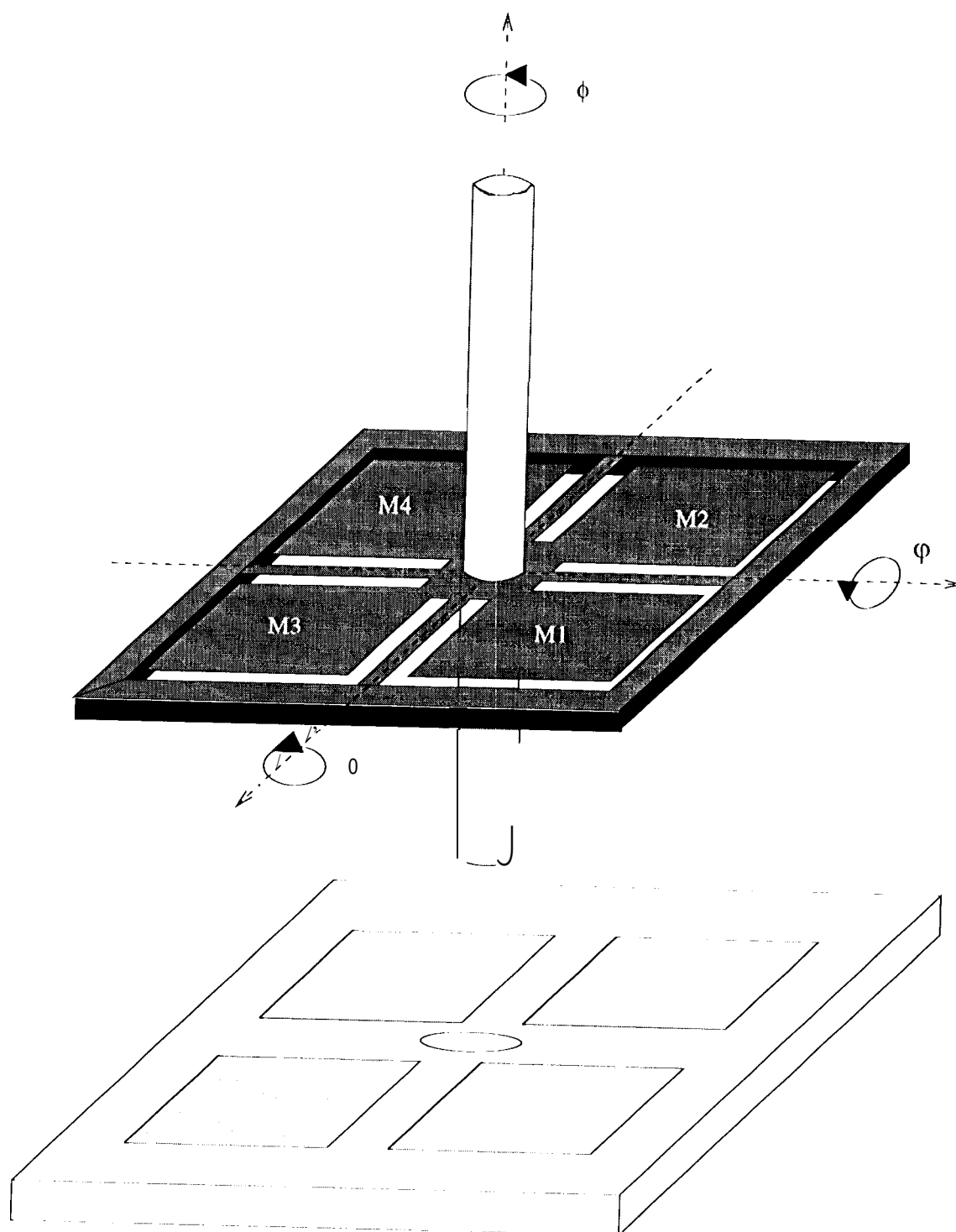
Figure 2-1: JPL/UCLA Micromachined Vibratory Gyroscope

$$I_\psi \ddot{\psi} + \alpha_\psi \dot{\psi} + \kappa_\psi \psi = Torque_\psi(\Omega_x, \Omega_y, \Omega_z, 0, \psi, \phi) \qquad (2.2)$$

$$I_\phi \ddot{\phi} + \alpha_\phi \dot{\phi} + \kappa_\phi \phi = Torque_\phi(\Omega_x, \Omega_y, \Omega_z, 0, \psi, \phi) \qquad (2.3)$$

Where I is the rotational intertia, α is the linear viscous loss coefficient, and κ is the sum of the displacement and torsional spring constants of the cantilevers in the given direction. Orders of magnitude for I and κ were found analytically based on the geometry of the structure and their values are given in table 2.1. These numbers were also validated by a finite element analysis model. Estimates have also been made for the neighborhood of α based on some simple fluid dynamics. These appear in the table as well. [5]

In general, simulations of the entire system have found that displacements around the ϕ axis are much smaller than either 0 or ψ. Also, the Coriolis forces which may result from vibrations of this mode and applied angular rates Ω_x and Ω_y are scaled by I_ϕ, which is an order of magnitude less than I_0 or I_ψ. Therefore, since this third degree of freedom is a stable mode that only negligibly affects the dynamics of the rest of the system or its output, it will be droped from the model, reducing the complexity and order of the model without signifigant cost.

2.2.2 Applied Forces

The torque function on the right hand side of each equation is a combination of the electrostatic driving force and the coriolis terms. The gyroscope is driven to vibrate on the 0 mode by the application of a voltage on the baseplate. The force and torque created by this voltage is given by

$$F = \frac{\epsilon_0 A}{d^2}[V(t)]^2 = \frac{\epsilon_0 A}{(d_0 + l_{arm}0)^2}[V(t)]^2 \qquad \mathbf{(2.4)}$$

$$M = Fl_{arm} \qquad (2.5)$$

l_{arm} is the effective orque lever, and can be estimated by the perpendicular distance from the axis node line to the center of the paddle. If $l_{arm}0$ is an order of magnitude less that d_0, its effect on the force is small, and the denominator can be approximated

to $d_0{}^2$

Under the influence of an applied angular rate along the z axis, a coriolis torque term is created along the ψ which is the cross product of the angular rate and the driving motion. This is given by

$$M_\psi = (2I_0\dot\theta)\Omega_z \tag{2.6}$$

This precession vibration wil create a feedback coriolis term in the θ direction, one again, Of

$$M_\theta = (2I_\psi\dot\psi)\Omega_z \tag{2.7}$$

This latter term is generally much smaller than the drive. However, it is the largest stray coriolis torque to appear from the theoretical equations. All others are negligible and are dropped. This means that the effects of Ω_x and Ω_y no longer figure into the model, making it unsuitable for predicting response due to tumbling conditions.

Note also that the displacements around ψ change the distance between the baseplate and paddles M1 and M2, used to drive vibrations along the θ axis. It is posssible to include this mechanism in the electrostatic forcing equation. However, ust as changes in θ were too small to consider, this effect is also ignored.

Therefore, the final, simplest possible equations for the dynamics Of the gyroscope can be given by

$$I_0\ddot\theta + \alpha_\theta\dot\theta + \kappa_\theta\theta = \frac{\epsilon_0 A l_{arm}}{(d_0)^2}[V(t)]^2 + (2I_\psi\dot\psi)\Omega_z \tag{2.8}$$

$$I_\psi\ddot\psi + \alpha_\psi\dot\psi + \kappa_\psi\psi = (2I_0\dot\theta)\Omega_z \tag{2.9}$$

2.2.3 Electronics

As stated in the Operation section, this gyroscope is both driven and sensed electrostatically. The changes in displacement causes changes in the capacitance between the baseplate and both M3 and M4. Therefore, if a constant bias voltage is applied

to the baseplate electrodes, a current will be generated.

$$I(t) = \frac{d}{dt}(CV) = V\frac{d}{dt}\left(\frac{\epsilon_0 A}{d_0 + l_a rm(\theta + \psi)}\right) \tag{2.10}$$

Completing the differentiation yeilds

$$I(t) = -V\epsilon_0 A\frac{\dot{\theta} + \dot{\psi}}{(d_0 + \theta + \psi)^2} = -V\epsilon_0 A\frac{\dot{\theta} + \dot{\psi}}{d_0^2} = K'_{out}(\dot{\theta} + \dot{\psi}) \tag{2.11}$$

for displacements where θ and ψ are small.

This current runs through a 1 MΩ bias resistor, and this voltage is then put through a voltage amplifier with a gain of 1000. Therefore, he preamp circuit has two outputs, on for each electrode.

$$V_1 = 10^9 K'_{out}(\dot{\theta} + \dot{\psi}) = K_{out}(\dot{\theta} + \dot{\psi}) \tag{2.12}$$

$$V_2 = 10^9 K'_{out}(\dot{\theta} - \dot{\psi}) = K_{out}(\dot{\theta} - \dot{\psi}) \tag{2.13}$$

These signals feed both differential and summing amplifier circuits. The differential amplifier subtracts the two, which is really a voltage representation Of the veloci ty Of ψ. For sinusoidal displacements, this is just the displacement with an amplitude gain proportional to the frequency and a quadrature phase displacement. This is the output signal Of the gyroscope.

The summing amplifier produces a voltage representation Of $\dot{\theta}$. This output is used to turn the gyroscope into a oscillator. The derivative is normalized and fed back as the drive signal, causing the gyroscope t 0 vibrate at the natural frequency Of the O mode. By placing a variable gain on this feedback signal and making this gain proportional to the integral Of the velocity amplitude error, it is possible to turn the gyroscope drive axis into a self oscillating system servoed a known $\dot{\theta}$. In other words, the input torque to the drive axis Of the gyroscope should be

$$v_{in} = \frac{K_i}{\dot{\theta}_0}\left(\int \dot{\theta}_0 - \dot{\theta}_{0DES}\right)\dot{\theta} \tag{2,14}$$

17

where

$$\dot{\theta}_0 = \frac{1}{2}\left(amplitude(V_1) + amplitude(V_2)\right) \tag{2.15}$$

Note that the torque on the gyroscope is actually proportional to the square of the input voltage. Therefore, only an attractive force can be applied to the baseplate. The v_{in} as is given above would be absoluted when applied, producing an incorrect drive. In actual operation, a DC bias of about 2 volts would be placed on the drive electrodes, and K_i must be set so that the drive is an AC signal around this voltage of about 4 Vpp. [4]

2.3 Summary of Final Theoretical Equations

The final theoretical equations Of the gyroscope after many simplifying assumptions becomes

$$I_0\ddot{\theta} + \alpha_\theta\dot{\theta} + \kappa_\theta\theta = \frac{\epsilon_0 A l_{arm}}{d_0^2}[V_{in}(t)]^2 + (2I_\psi\dot{\psi})\Omega_z \tag{2.16}$$

$$I_\psi\ddot{\psi} + \alpha_\psi\dot{\psi} + \kappa_\psi\psi = (2I_\theta\dot{\theta})\Omega_z \tag{2.17}$$

For the electronics, if V_1, V_2 and θ_0 are defined as in section 2.2.3

$$V_{in} = K_i\left(\int \dot{\theta}_0 - \dot{\theta}_{0DES}\right)\frac{\dot{\theta}}{\dot{\theta}_0} + 2V \tag{2.18}$$

$$V_{out} = K_{out}(amplitude(V_1) - amplitude(V_2)) \tag{2.19}$$

These formulas gave the microgyroscope team a framework for expected behavior and magnitudes of various responses. However, since the theoretical model upon which this was based was entirely ideal and nongeneralized, it was assumed that experimentation would be needed to refine the predicted values. This next section is a breif description of the preliminary testing of prototype gyroscopes to validate the above equations.

Chapter 3

Testing Procedures and Results

Development work on the JPL/UCLA microgyroscope began in January 1995. In the spring of that year, i was chosen to be a flight experiment on the Mars Explorer/Pathfinder mission scheduled for launch by the end of 1996. Consequently, the project has been greatly accelerated in the effort to build a working device before the deadline. So far, severa prototype gyroscopes ave been assembled and tested. Their physcial parameters are slightly varied in order to analyze for possible rules of optimization Unfortunately, this makes he idea of sta istical analysis to develop an empirical model an impossibility. However, t is still possible to examine trends in all the gyroscopes to substantiate the validity of the model presented in the previous chapter.

3.1   Testing and Characterization Procedures

Three preliminary testing procedures and two test centers have been developed to characterize the microgyroscopes. They are breifly described in the sections below.

3.1.1   Frequency Response Testing

The first testing center is devoted exclusiely to determining static characteristics, such as mode shapes and resonant frequencies. The testing facility is shown schematically

TOP VIEW

(Into Optical Window)
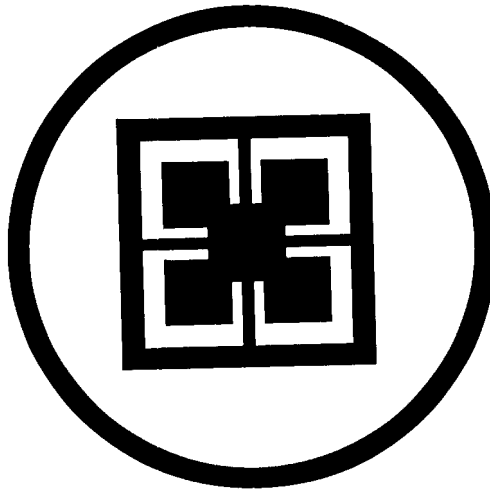
SIDE VIEW

(Entire Testing Station)

Interferometer

Spectrum

" , , , , " c

Phase Lock-In
Analyzer

Laser

Window

Signal
Generator

Micro-
Manipulator

Vacuum
Chamber

Gyro

Isolation Table

Computer
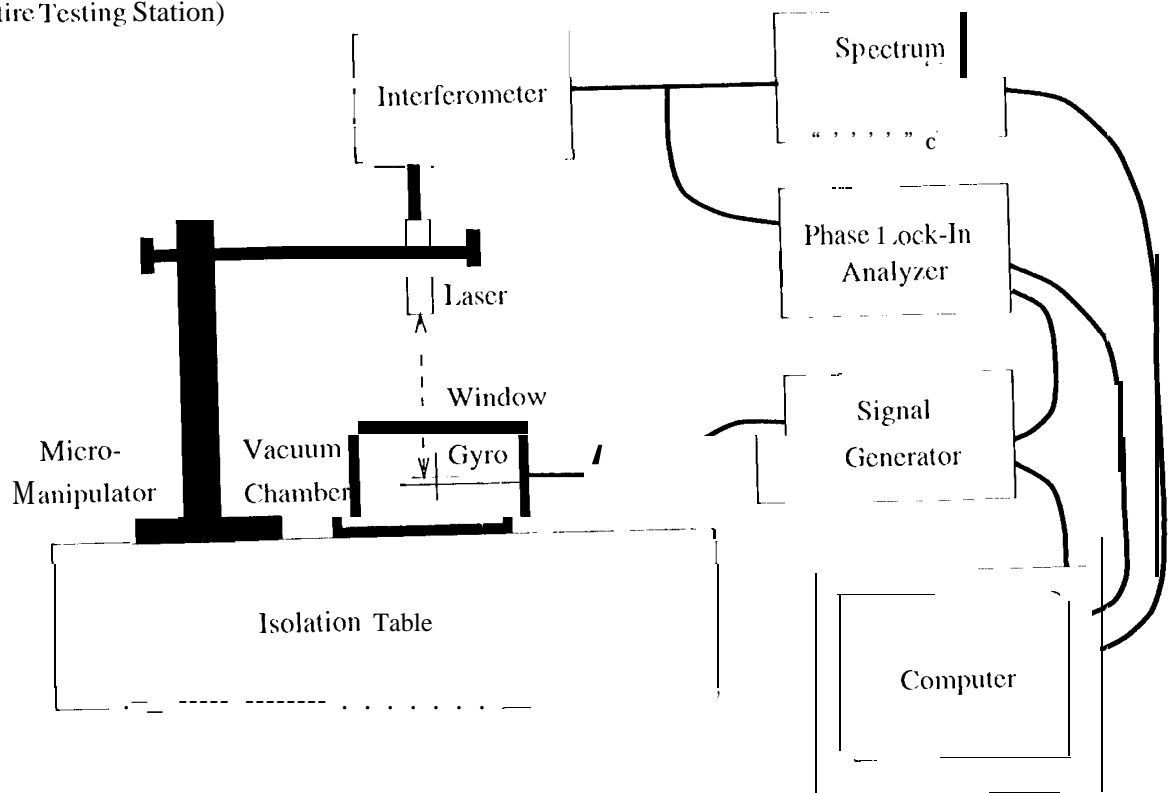
Figure 3-1: Static Characterization Testing Station

in figure 3-1. The gyroscope is placed in a small vacuum chamber (about 50 mTorr) with a sealed optical window above it and four electrical probe feedthroughs. The chamber is grounded. The gyro element (post and paddles) is grounded to the chamber. Each Of the probes is attached to one Of the electrodes, allowing each plate to be controlled individually. A laser interferometer, mounted onto a micromanipulator which allows movement in the x, y and z axises as well as small angular rotations, is positioned over the window, so that it can measure movement Of any point on any Of the gyroscope paddles. The entire assembly is secured to a pneumatic isolation table.

The inputs to the gyro are fed by either a signal generator or white noise from a dynamic signal analyzer. The output Of the laser interferometer is passed through both the dynamic signal analyzer, and a phase lock-in analyzer referenced by the signal generator output. Both analyzer outputs are then fed to a computer running a Visual Basic application specifically written for these tests. All the instrumentation is also computer controlled over a GPIB bus. Eventually, the micromanipulator will have GPIB controllable actuators, and all the procedures for this test will be computer controlled. Unfortunately, at this time, the operator must still position the laser interferometer himself.

Two separate tests can be run in this station. First, white noise is applied to one of the four paddles, and the interferometer is placed above it to measure displacements. The output goes to the dynamic signal analyzer which calculates the spectrum Of the signal normalized by the white noise. This test can be used to pinpoint resonant frequencies, which, in vacuum, appear as sharp peaks in the spectrum. Generally, there are three peaks, one for the drive resonance, one for sense resonance, and one for the "bounce" mode, where the entire gyro element is translating along the z axis. The bounce mode resonant frequency is generally much higher than the rotational resonances.

Once the resonances are determined, the input is switched from white noise to the signal generator, which is tuned to one Of those frequencies. The interferometer is then swept across the area Of the gyro paddles, and the magnitude Of the peak at each position is recorded. These values are then plotted two dimensionally as a
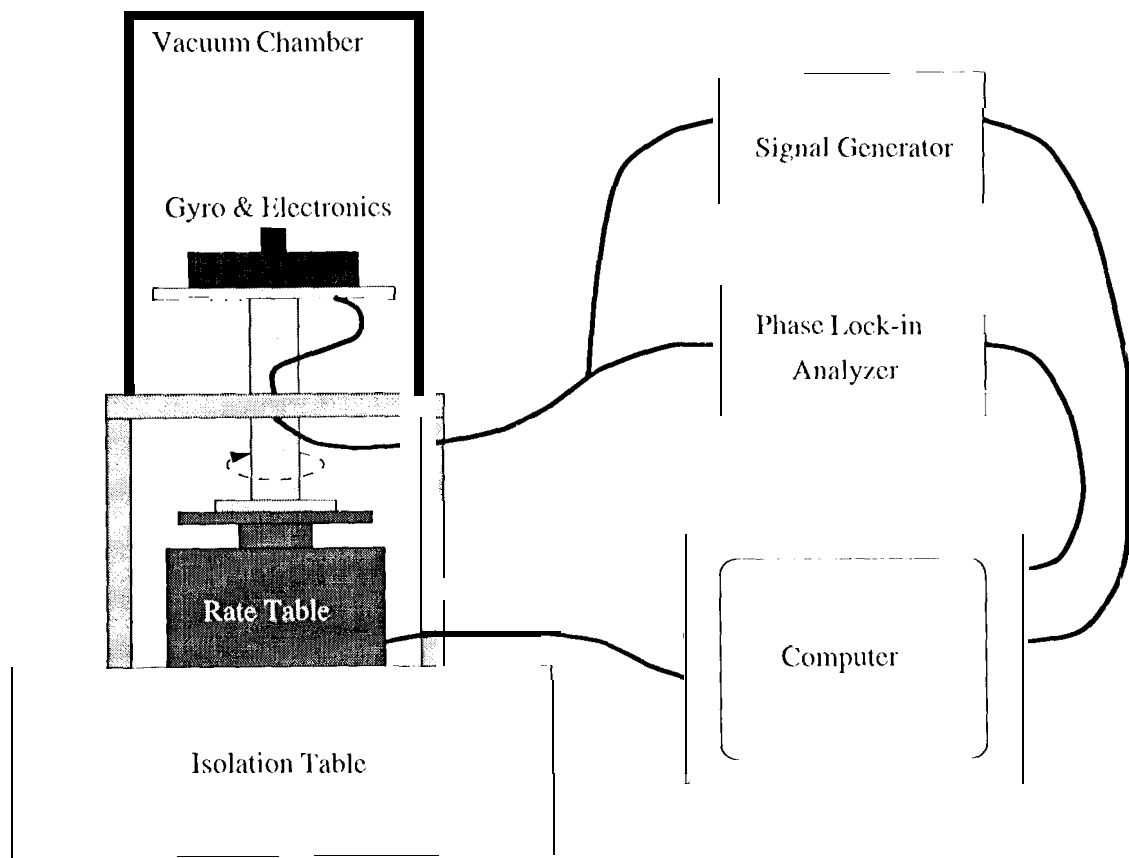
Figure 3-2: Dynamic Characterization Testing Station

function Of position to produces a picture of the mode shape. The test is repeated for each resonant peak found in the spect rum. This way, the shape of each mode can be quickly determined. Once laser positioning is automated, the static characteristics Of any prototype gyro can be found in record t ime wit h the touch Of button. If desired, the results Of one test group can be verified by applying the inputs to a different paddles. The end reults, resonant frequencies and mode shapes, should be identical.

3.1.2 **Rotational** Testing

The other two trots are both performed on the same station which is shown schematically in figure 3 - 2 . The gyroscope and preamplifier circuit are placed in a larger vacuum cha mber (agai n, about 50 mTorr), at op a platform which is mounted to a

rotary vacuum feedthrough. Outside the vacuum, this feedthrough is driven by a precesion rate table. Th e re are also electronics feedthroughs which are connected to power, the drive inputs, and the sense outputs within the chamber. Outside the chamber, the drive input is fed by another signal generator, and the sense outputs are fed to another phase lock-in analyzer. The table and the instrumentation are once again all computer controlled.

The table can be set to rotate at sp eeds Of ±0.01 deg/sec u]) to ±99.99 deg/sec via a DC voltage input. In this way, the computer can set the applied angular rate to any speed i n the above range and automatically record the gyroscope response. A testing algorithm has been set up were the operat or chooses a start angular rate, and end angular rate, and the number O f poin ts between these two values. First, the computer calculates the series Of angular rates the operator has requested. Then the table is spun at the start rate for a length Of time, depending on the current integration time constant Of the Of the phase lock-in. A t the end of this period, the computer records a seris Of voltage measurements. Then, it stops the table for the same length Of that it was rot at ing, and records the bias volt age. Afterwards, it goes on to next rate and repeats the process. In this way, it is possible to determine the reponsivity and threshold, and the bias voltage during testing. An example of a plot produced by this testing is shown in figure 3-3.

3.1.3 Allan **Variance** Testing

The fills] type Of preliminary testing performed 011 these prototype gyroscopes w a s an Allan variance test, a statistical method which is used in the gyro community to determine noise characterist ics. The output is a Green chart, which can be used to determine the resolution as a function Of the averaging time constant (7) Of the sensing circuit. The gyro and electronics are once again in the same large chamber. I lowever, they are not rotated. Therefore, the only possible applied angular rate is earth rate, which can be assumed to be constant. The output is sampled and integerated to

Nomenclature	Rate AV Slope	Angle AV Slope	Rate PSD Slope	Angle PSD Slope
White Angle	$\frac{1}{2}$	-1	0	+2
Angle Quantization	0	-1	0 -	+2
Flicker Angle	o	-1	0	+2
Angle Random Walk White Rate Noise	-1 $\frac{1}{2}$	$\frac{1}{2}$	-2	0
Rate Quntization	+1	0	-2	0
Bias Rate Instablilty	+1	0	- 3	-1
Rate Random Walk	+ 1 $\frac{1}{2}$	-1 $\frac{1}{2}$	-4	-2

Table 3.1: Properties of Noise Sources in an Allan Variance Plot

determine angle and then passed through the rate Allan variance algorithm

$$0(t) = \int^{t} \Omega(t')dt' \qquad (3.1)$$

$$\dot\Omega_k = \frac{0(t_k + \tau) - 0(t_k)}{\tau} \qquad (3.2)$$

$$\sigma_\Omega^2 = \frac{1}{2}(\dot\Omega_{k+1} - \dot\Omega_k)^2 \qquad (3.3)$$

111 other other words, the stationary gyro output is sampled at some high (1 kHz) rate. Each sample is then added to the angle integral which makes up the Previous history of the test. The angle average is computed for a series of increasing time constants τ, generally powers of 2 to simplify the computation program, to create an Allan variance plot, or a Green chart. By examining the slopes Of the plot at various intervals Of τ, it is possible to determine what type Of noise dominates for any specific integration constant. [2] Some Of the more common noise sources are listed in Table 3.1.

24

Gryroscope ID Number	1 St Resonance	2nd Resonance	3rd Resonance
Theoretical	300"- 500Hz	300"-500"1 Iz	400"-600" Hz
XP-9	293.0 Hz	405.0 Hz	463 Hz
XP-15	396.8 Hz	436.6 Hz	513.0 Hz
XP-16	589.1 Hz	596.1 Hz	714.0 Hz
XP-23	439.0 Hz	444.4 Hz	569.0 Hz

Table 3.2: Sample Gyroscope Resonant Frequencies

Allan variance analysis can also be done on the angle, by integrating the data twice and the basically following the same procedure. In order to differentiate between certain types of noise, it is often necessary to also look at the PSD of the gryoscope. However, given some insight into the system itself, it is possible to develop a preliminary a model of the noise just from the actual data of the Green chart itself. The PSD plots and the information in table 3.1 would definitely be needed, however, once even better models with more refined noise algorithms are required.

3.2 Test Results

The model was correct in characterizing the gyroscope as a second order resonant system. Table 3.2 shows values for resonances for the tested prototype gyroscopes. Typical ranges predicted by the theoretical model are also given. Except for the unsurprising fact that the drive and sense axis were never exactly equal, there was reasonable agreement between the expected and actual results.

A sample of the rotation testing from XP-23 is given in figure 3-3. The responsivity of this gyro was about 1.25 mV / (deg/sec) Some prototypes were close to 2 mV /(deg/sec). As predicted, the response was always linear with respect to the applied angular rate. The threshold was about 0.05 deg/sec, and the resolution with the current electronics about 0.1 deg/sec.

Finally, a sample of a Green Chart from the same gyroscope if given in figure 3-4. For the theorectically ideal gyroscope, the line would have been flat. However, for
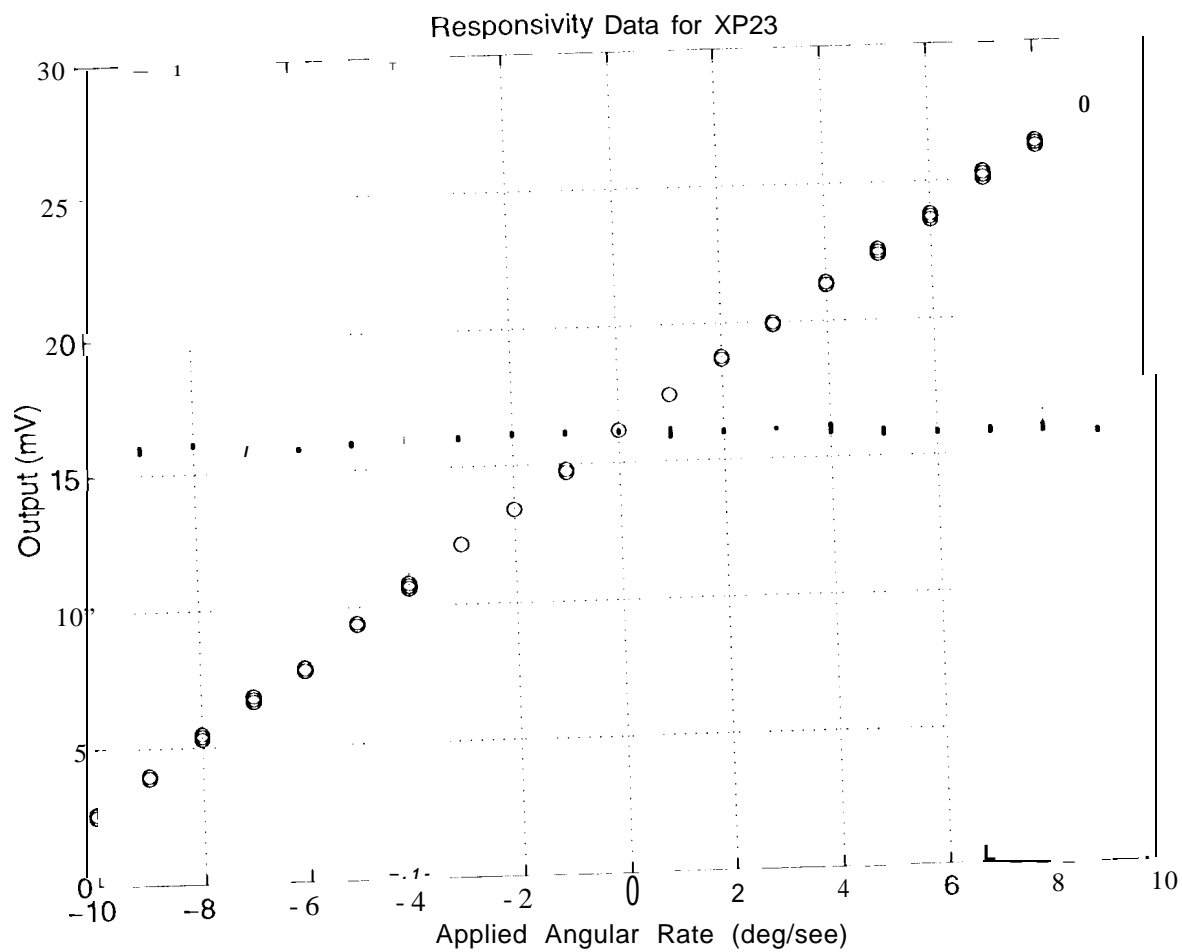
Figure 3-3: Responsivity Data for XP-23, 4 Volt p/p drive.
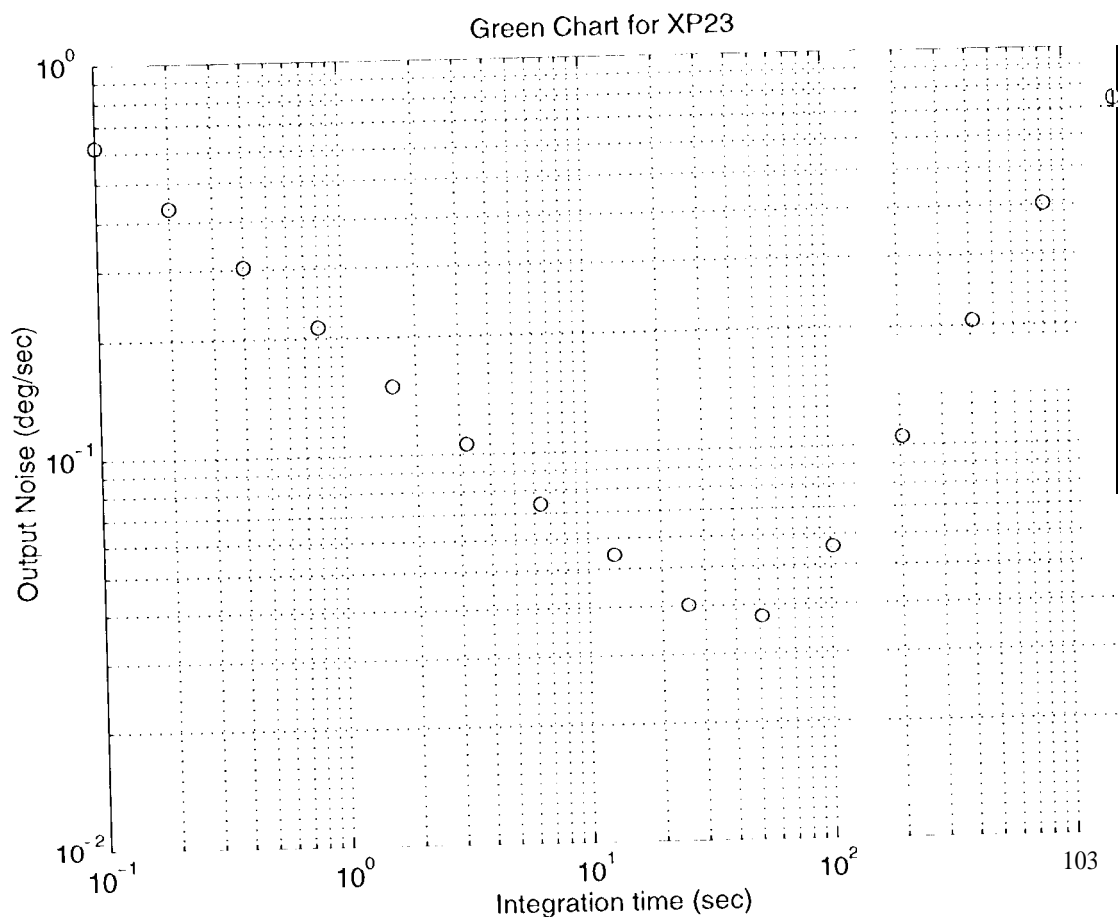
Figure 3-4: Green Chart for XP-23

faster time constants, the line has a slope Of $-\frac{1}{2}$ suggesting angle measurement noise. And, at slower time constants, there is a slope Of -1 1, suggesting either bias rate instability or rate quntization noise. All are random effects which must somehow be incorporated into the theory.

Several trends observed from this data validated the theory. However, many behaviors were not predicted by the model. For example:

1. The resonant frequencies Of the drive and sense axis were not the same.

2. The resonant frequencies tended to drift randomly with time.

3. There was an offset bias signal whose value also drifted randomly with time.

4. The Allan variance data showed that angle white noise was the dominant noise factor for integration times of less that 10 seconds while rate bias instability was dominant for integration times greater that 100 seconds.

The model should be refined to include these errors. This means that physical explanations need to be presented as to their sources, so that, while they may never be completely removed, they can be designed against, further improving the gyroscope resolution. Also, once understood, they can be incorporated into a new model which can be used to test out signal processing schemes or evaluate performance in specific applications.

One final note must be made. At the time of the tests above, the summing amplifier and oscillator circuits were not in place. The drive voltage was provided by a signal generator running at the measured sense resonant frequency, and periodically adjusted as that frequency drifted. Therefore, it is safe to assume the amplitude of $\dot{\theta}$ was constant during a given data acquisition session. However, the actual value of θ is unknown, leaving unfortunate gaps in the test data for the prototypes. The effects of this lack on the model are discussed in the following chapters.

Chapter 4

Vibratory Gyroscope Errors

Most of the shortcomings of the model lie in two areas. First, it assumes that the mass is perfectly balanced and perfectly symmetrical about the radial and lateral axis. In reality, because of manual assembly and the glueing process, there are small mass imbalances about the radial axis, which have a signifigant impact on the drive path of the post. Secondly, it ignores all time varying affects outside of the desired inputs, i.e. drive forces and applied angular rates. This is also invalid.

4.1 Mechanical Cross Coupling

The largest and most common source of mechanical error in vibratory gyroscopes is mechanical cross coupling. An unbalanced mass element couples the drive enery into and consequently creates displacements along the sense axis. Consider the free body diagram shown in figure 4-1. For a perfectly balanced gyro element, the kinematic equations (in the absence of coriolis force) can be described by the following matrix equation.

$$T = I\ddot{u} + A\dot{u} + K u \qquad (4.1)$$

01"

$$\begin{bmatrix} \tau_\theta \\ 0 \end{bmatrix} = \begin{bmatrix} I_\theta & 0 \\ 0 & I_\psi \end{bmatrix} \begin{bmatrix} \ddot{\theta} \\ \ddot{\psi} \end{bmatrix} + \begin{bmatrix} \alpha_\theta & 0 \\ 0 & \alpha_\psi \end{bmatrix} \begin{bmatrix} \dot{\theta} \\ \dot{\psi} \end{bmatrix} + \begin{bmatrix} \kappa_\theta & 0 \\ 0 & \kappa_\psi \end{bmatrix} \begin{bmatrix} \theta \\ \psi \end{bmatrix} \qquad (4.2)$$

29
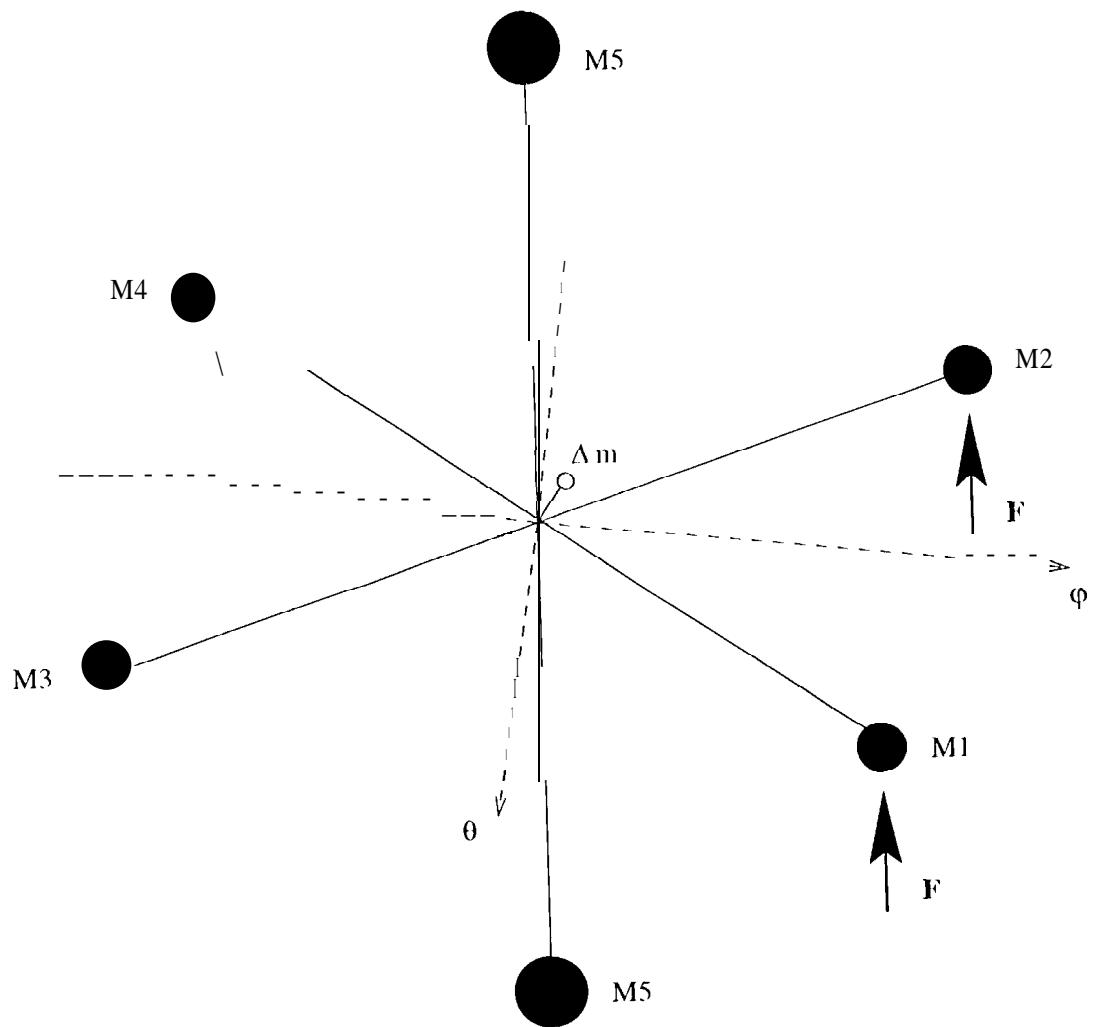
Figure 4-1: Free Body Diagram of Gyroscope

The input vector τ is the effective torque produced by the electrostatic force applied to the two drive paddles. It is easy to see that multiplying out the above matrixes will produce equations 2.16 and 2.17. when there is no applied angular rate.

The presence Of the imbalance mass has a double effect. First, it changes the inertia tensor I, so that the cross product terms are no longer 0. Secondly, the moment arms Of the forces F_{M1} and F_{M2} from the individual drive paddles are no longer equal, meaning that the drive force wil now have a component in the ψ direction. Therefore,

$$I' = \begin{bmatrix} I_0 & \Delta I \\ \Delta I & I_\psi \end{bmatrix} \qquad\qquad \tau' = \begin{bmatrix} \tau_0 \\ \Delta\tau \end{bmatrix} \tag{4.3}$$

The new equations Of motion are given by

$$\tau = I_0\ddot{\theta} + \Delta I \ddot{\psi} + \alpha_0\dot{\theta} + \kappa_0\theta \tag{4.4}$$

$$\Delta\tau = I_\psi\ddot{\psi} + \Delta I \ddot{\theta} + \alpha_\psi\dot{\psi} + \kappa_\psi\psi \tag{4.5}$$

in general, τ exerted by the electrostatic drive is much greater than $(\Delta I)\ddot{\psi}$ allowing the latter term to be dropped. Rearranged into a more familiar form, the above equations become

$$I_0\ddot{\theta} + \alpha_0\dot{\theta} + \kappa_0\theta = \tau \tag{4.6}$$

$$I_\psi\ddot{\psi} + \alpha_\psi\dot{\psi} + \kappa_\psi\psi = \Delta\tau + \Delta I \ddot{\theta} \tag{4.7}$$

The right hand side Of the last equation is the cross-coupled torque exerted on the sense axis solely due to drive motion. This error is commonly referred to as a "zero signal" in gyro literature, since a signal for angular rate is being produced even though zero angular rate is being applied. When the structure is being driven on resonance, τ and $\Delta\tau$ are in phase with the velocity of the drive displacement $\dot{\theta}$. The acceleration $\ddot{\theta}$, on the other hand, is in phase with θ itself. Therefore, this torque can be rewritten as

$$M_{cc}(\theta - \} \psi) = 2I_0\left[\Omega_q(t).\theta + \Omega_d(t).\dot{\theta}\right] \tag{4.8}$$

31

Expected Path   Actual Path

(no displacement   (displacement on both
on φ axis) θ axis and φ axis)
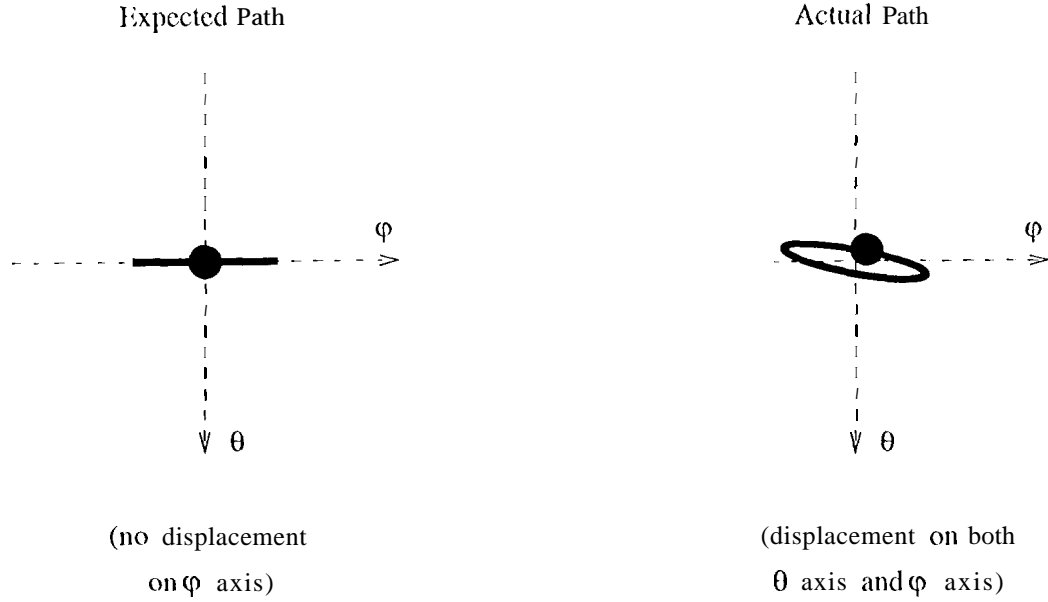
Figure 4-2: Expected and Actual Path of Mass Element

Where the first term on the right hand side is due to the reaction forces from the resonant structure and would be in quadrature with any coriolis torque signal. The second term is due to the drive forces themselves, and would be in phase with a coriolis signal. Figure 4-2 shows the expected versus actual path Of the post as seen from above. Balance imperfections will actually cause the post to wobble slightly, resembling the precession caused by a coriolis force.

For the geometry shown in figure 4-1, it is easy to calculate the magnitudes Of the two cross coupled torques in terms Of Δm, its displacement from the θ axis, x, and the displacement from the ψ axis, y. Once again, assuming that the gyro is begin driven On its drive resonance

$$\Omega_q \theta = \Delta m x y \ddot{\theta} = \Delta m x y \omega_\theta^2 \theta \tag{4.9}$$

$$\Omega_d \dot{\theta} = Fx = \left(\frac{\kappa_\theta}{Q_\theta} \theta \right) = \frac{\kappa_\theta x}{Q_\theta} \theta \tag{4.10}$$

32

$$\frac{\Omega_q 0}{\Omega_d \dot{0}} = \frac{1}{\kappa_\theta} \Delta m y \omega_\theta{}^2 \qquad\qquad (4.11)$$

The last ratio is expected to be much greated than 1 for a macromachined post glued into place. However, it is impossible to calculate an exact figure without knowing Δm or y. The ratio is best found by experimentation.

Mass imbalances can also create errors in other ways. For example, if the gyro is actually made to tip over slightly, causing the initial displacements between the paddles and baseplate electrodes to be unequal, and driving will again result in a zero signal. There are also other kinds of imbalances. For example, the spring constants between the four cantilevers may not match. However, none of these additional perturbations will change the basic form of equation 4.8. They will all be in phase with either the displacement or the velocity of the drive. [3]

4.2 Time Varying Effects

If the zero signals discussed above remained constant over time, thenthey ('0111(1 be easily calibrated out of the gyro and not given much thought. Unfortunately, their magnitudes vary over time. in fact, it is the rate of variation of the zero signals which may limit the resolution of vibratory gyroscopes to any where from 3 to 6 orders of magnitude from its resolution otherwise. [1]. There are three typical mechanisms for time varying zero signal. They can affect the actual brass post, the silicon paddles and supports, or the glue used in assembly.

4.2.1 Non-uniform Creep

Creep occurs when a structure is strained cyclicly at high temperatures for extened periods of time. Even if these strain levels are in the elastic regime, plastic deformation can set in, changing the balance of the masses. Creep may indeed be a problem, since the post and especially the glue is being strained cyclically, and, under vacuum where heat dissipation is low, high thermal concentrations can be attained.

4.2.2 **Non-uniform Thermal Expansion**

As stated above, heat dissipation is extremely inefficient in vacuum. In addition to creep, the mass elements, supports, and the adhesive will also undergo non-uniform thermal expansion. Especially in the case Of the glue, which is applied non-uniformly by hand, small changes in volume can completely alter the mass balance. of the post by actually tilting the post itself.

4.2.3 **Non-uniform** Deflections **Under Acceleration**

This last possibility was most possibly not a factor in the testing performed (m the prototype gyros. However, it will be a factor in the function Of the gyros in real applications. In a theoretically balanced gyro, acceleration of the instrument frame would be a common mode signal on both sense electrodes which would then be subtracted out. However, if there is a mass imbalance, this signal will not be even on both sense pads, creating a zero signal which will change as the acceleration changes. It may be possible to know the acceleration from other instruments and somehow compensate for this effect. However, since the actual mass imbalance formula will be generally unknown, this may prove to be a challenge.

4.3 **Differential Frequency Drift**

The resonant frequency Of the driving and sensing systems should theoretically be equal, if the gyro is symmetric and its parameters time invariant. Unfortunately, neither Of these conditions is true. The resonant frequency Of a second order mass-spring system is given by

$$\omega_n = \sqrt{\frac{I}{\kappa}} \tag{4.12}$$

As seen from the discussion above, the effective I of each mode is definitely changing with time as the mass balance changes. It is also likely that κ which is a function Of the geometry, compliance, and prestress conditions Of silicon cantilevers, is also changing with time. These changes are partly due to some of the time varying effects

described above, but also partly due to stochastic effects that can only be modelled statistically.

Since the drive is an oscillator, it will track this changing frequency and continue to servo to the correct amplitude with a minimum energy expenditure. The major error caused by a shift in resonant frequency is a phase shift in the output of the sense. The phase angle error is given by

$$\angle \theta(\Delta\omega) = \angle G_{s.c.}(j\omega_c) `` \angle G_{s.c}(j\omega_c + j\Delta\omega) \tag{4.13}$$

If the sense circuit is not phase sensitive, this may not be much of an issue. However, as seen in previous sections, if the sense circuit is not phase sensitive, greater errors would occur.

In general, the prototypes gyros that were tested had resonances separated by at least a few hertz and high and narrow resonant peaks that did not overlap. However, at least on one gyro that underwent static characterization, it was seen that the peaks for the drive and the sense drifted towards each other, overlapped, and drifted apart, creating potentially fatal phase shifts on the output. This gyro would most possibly not be useful. However, even in gyros were the peaks seemed spaced widely apart, the phase shift still exists, and, as the sensing electronics improve, could pose some problems.

4.4 Damping Drift

For the JPL/UCLA microgryoscope, the damping is sensitive to Pressure. While pressure fluctuations may not be a problem for space applications, it may come up if the gyroscope is ever to be used in automobiles or aircraft. It is desirable to operate under the lowest possible pressure to achieve the greatest resonant amplification. However, the lower the pressure, the more difficult the vacuum is to maintain. Therefore, these effects should also be modelled.

4.5 Final Time Varing Model

In order to incorporate these changes easily into the model, it may be convenient to alter the form slightly from that given at the end of Chapter 2. A second order system as a transfer fucntion in the frequency domain of

$$\frac{\theta(s)}{Torque(s)} = H(s) = \frac{\theta_{DC}\omega_n^2}{s^2 + \frac{\omega_n}{Q}s + \omega_n^2} \tag{4.14}$$

where θ_{DC} is displacement of θ for a unit of torque and Q is the amplification of the amplitude of θ under resonance. In this model, both ω_n and Q can independently be described as functions of time. The final step is to include the cross coupled torque equation 4.8 into the torque fucntion on the sense. Therefore, the final time varying mechanical equations for the gyroscope are given by

$$\ddot{\theta} + \frac{\omega_{\theta n}(t)}{Q(t)}\dot{\theta} + \omega_{\theta n}^2(t)\theta = \omega_{\theta n}^2\theta_{DC}\left[\frac{\epsilon_0 Al_{arm}}{d_0^2}V_{in}^2(t) + 2I_\psi\dot{\psi}\Omega_z\right] \tag{4.15}$$

$$\ddot{\psi} + \frac{\omega_{\psi n}(t)}{Q(t)}\dot{\psi} + \omega_{\psi n}^2(t)\psi = \omega_{\psi n}^2\psi_{DC}\left[2I_\theta\dot{\theta}\Omega_z + 2I_\theta\Omega_q(t)\theta + 2I_\theta\Omega_d(t)\dot{\theta}\right] \tag{4.16}$$

The sum Of magnitude Of $\Omega_q(t)$ and $\Omega_d(t)$ can be determined from the Green chart for a particular prototype gyroscope. Unfortunately, at the present time, tests and electronics have not been developed to determine $\Omega_q(t)$ and $\Omega_d(t)$ separately, s i n c e the actual displacement function Of θ is unknown. At the present time, they will be varied so that their sum remains in the neighborhood of the test d a t a .

The electrical equations, notably the output equation, must also be changed. The Allan variance suggests that there is an angle measurement error. Therefore, the function for V_{out} is now given by

$$V_{out} = K_{out}[amplitude(V_1) - amplitude(V_2)] + noise(t) \tag{4.17}$$

Chapter 5

System Simulation

The model given in the previous chapter is just a series of ordinary differential equations. A simple C program can be used to simulate their behavior for arbitrary inputs over a given interval of time. However, first the actual functions for each of the time varying parameters for a particular gyroscope must be determined. For this report, a model will be created to simulate the behavior of the prototype XI '-23.

5.1 Calculation of Parameters

5.1.1 Empirical Constants and Measurements

Tables 5.1 and 5.2 are listings Of all the paramters that can be measured directly, including the entire geometry Of the gyro, and the electrical circuit properties. Some Of these numbers will need to be used to calculate values in the experimetally determined model.

Unfortunately, the testing procedures developed so far cannot completely characterize the prototype gyroscope parameters. Therefore, the theoretical values for the ideal moment of inertia and restoring force still need to be known. The restoring force comes from deflection Of the cantilever supports, and the formula is derived from simple beam theory. Its value is $\kappa_\theta = \kappa_\psi = 2.71 \times 10^{-4} \frac{N \cdot m}{rad/sec}$. The moment of iner ia of the entire gyro element can be approximated by the inertia of the post,

37

Parameter	Value	Constant	Value
Post diameter	0.45111111		
Post length	5.00 111111	Brass Density	19000 $\frac{kg}{m^3}$
Paddle side	1.50111111		
Spring length	1.25 111111		
Spring width	26.(K) μm	Si Youngs Modulus	1.9X $10^{11} \frac{N}{m^2}$
Spring depth	26.00 μm		
Center square width	1.75 mm		
Electrostatic lever arm	1 .(N mm	Si Bulk Modulus	7.3x $10^{10} \frac{N}{m^2}$
Seperation space	10 μm		

Table 5.1: Empirically Determined Physical Paramters fpr XP-23

Parameter	Value	constant	Value
Bias Voltage	4 V		
Bias Resistance	1 MΩ	ϵ_0	$8.85 \times 10^{-12} \frac{F}{m}$
Preamplifier Gain	'1 000		

'able 5.2: Empirically Determined Electrcal Parameters for XP-23

which is aslo a simple problem. $I_\theta = I_\psi = 3.17 \times 10^{-11} \frac{Kg}{m^2}$.

5.1.2 DC Displacement

The largest hole in the empirical information on the gyroscope is the DC displacement of θ or ψ due to a unit force. Therefore, it is assumed that θ_{DC} is the theoretical displacement for the calculated restoring force.

$$\theta_{DC} = \frac{1}{K_\theta} = 3.69 \times 10^3 = \frac{1}{K_\psi} = \psi_{DC} \tag{5.1}$$

5.1.3 Electronic Gains

The electrostatic force is being applied on two paddles. This force is then converted to a torque around the drive axis through the lever arm. Therefore, the gain on the voltage input is

$$M = \theta_{DC}\omega_{\theta n}{}^2(t) \left[\frac{2\epsilon_0 A l_{arm}}{d_0{}^2}\right] V^2(t) = \theta_{DC}\omega_{\theta n}{}^2(t) K_{in} V^2(t) \tag{5.2}$$

0 1

$$M = \theta_{DC}\omega_{\theta n}{}^2 K_{in} V^2(t) = (6.33 \times 10^3)\omega_{\theta n}{}^2(t) \times (3.98 \times 10^{-10}) V^2(t) \tag{5.3}$$

The output gain equation is similar to that of the input gain. However, it is al so scaled by the bias voltage, the bias resistance and the preamp gain. From the values given in table 5.2 this comes to either $K_{out} = 1.593$.

5.1.4 Physical Parameter Drifts

In this form of the second order equation, there are only two parameters t hat drift, the resonant frequency ω_n and the! peak amplification factor Q. Both Of these effects were qualitatively observed during the testing procedure. The drive resonance Of XI'-23 centered around 4391 lz and the sense resonance around 444 Hz. A smooth drift

of at most 0.5 Hz a minute was observed, but the two resonances never really moved more than 2 Hz away from these centers.

'1 'he peak amplification was measured by comparing the output of the gyro when driven off resonance, to when it was driven on resonance. This amplification was found to be between 50 to 100.

5.1.5 **Verification of** Responsivity

It is possible to verify that the above estimates of the physical parameters are acurate through hand calculations using the experimental reponsivity. First assume that the resonant amplification Q = 75. If the drive mode would have this is the amplification for a sinusoid at 439 Hz, then the amplification at 444 Hz (the sense resonance, where it was actually driven for this data) is about 28. Therefore, the magnitude of the velocity of the drive vibration is

$$\dot{\theta}_0 = \omega_\psi \theta_0 = \omega_p si Q_{\theta at\psi} \omega_p si \theta_{DC} \omega_\theta^2 K_{in} V_0^2 = 1.84 \tag{5.4}$$

which means that for a angular rate of 1 $\frac{deg}{sec}$, the change in coriolis torque is given by

$$M_0 = 2I_\theta \dot{\theta}_0 \Omega_z = 2.03 \times 10^{-12} \tag{5.5}$$

This should result in a sense velocity magnitude of

$$\dot{\psi}_0 = \omega_\psi \psi = \omega_\psi (Q \psi_{DC} M) = 1.5709 \times 10^{-3} \tag{5.6}$$

Finally, this should produce a change in output of

$$V_{out} = K_{out} \dot{\psi}_0 = 2.5mV \tag{5.7}$$

The actual reponsivity is about half that, suggesting that some of values used above were calculated/esti mated on the high side, especially in the case of Q. If the Q were actually 50, the same process would yeild a reponsivity of 0.6 mV. The fact that there

was order of magnitude agreement suggests that it is safe to proceed.

5.1.6 Angle Measurement Noise Magnitude

According to the Green Chart of XP-23, the dominant error for integration time constants equal to or lower than 10 second is angle measurement error. This is essentially the trace wid.h of the signal, and is probably attributable to thermal fluctuations in the circuit. It can be simulated by adding a random number within the magnitude specified by the data, to the final output.

$$N_k(mV) = \frac{0.02745}{\sqrt{\tau}} \tag{5.8}$$

Where τ is the total averaging time of .he sense circuit. This line is shown in the first plot in figure 5-1 against the actual data in millivolts.

5.1.7 Cross Coupling Magnitude

A oove an averaging time of 100 seconds, rate bias instability is probably .he dominant noise source. t can be seen from chart recorder outputs that the bias tends to grow steadily in one direction over time, even for a period of minutes. The asymptote in this region is given by

$$\Omega_d \cdot \Omega_q = -\left(5.127 \times 0^{-4}\right) \tau \tag{5.9}$$

This line is shown against the data in the second plot of figure 5-1. The sugggestion is that if a gyro with this noise characteristic were left perfectly still for a full second, it would still believe that it had experienced an average rate of $5.127 \times 10^{-4 \frac{deg}{sec}}$. So if the bias had begun at 0, at the end of one second, that bias would be indicate a rate of $10.34 \times 10^{-4 \frac{deg}{sec}}$. This can be modelled as the rate of change of the zero-signal discussed in the previous chapter, since any mechanical *cross-coupling* would be manifest itself in the rate output as a bias.
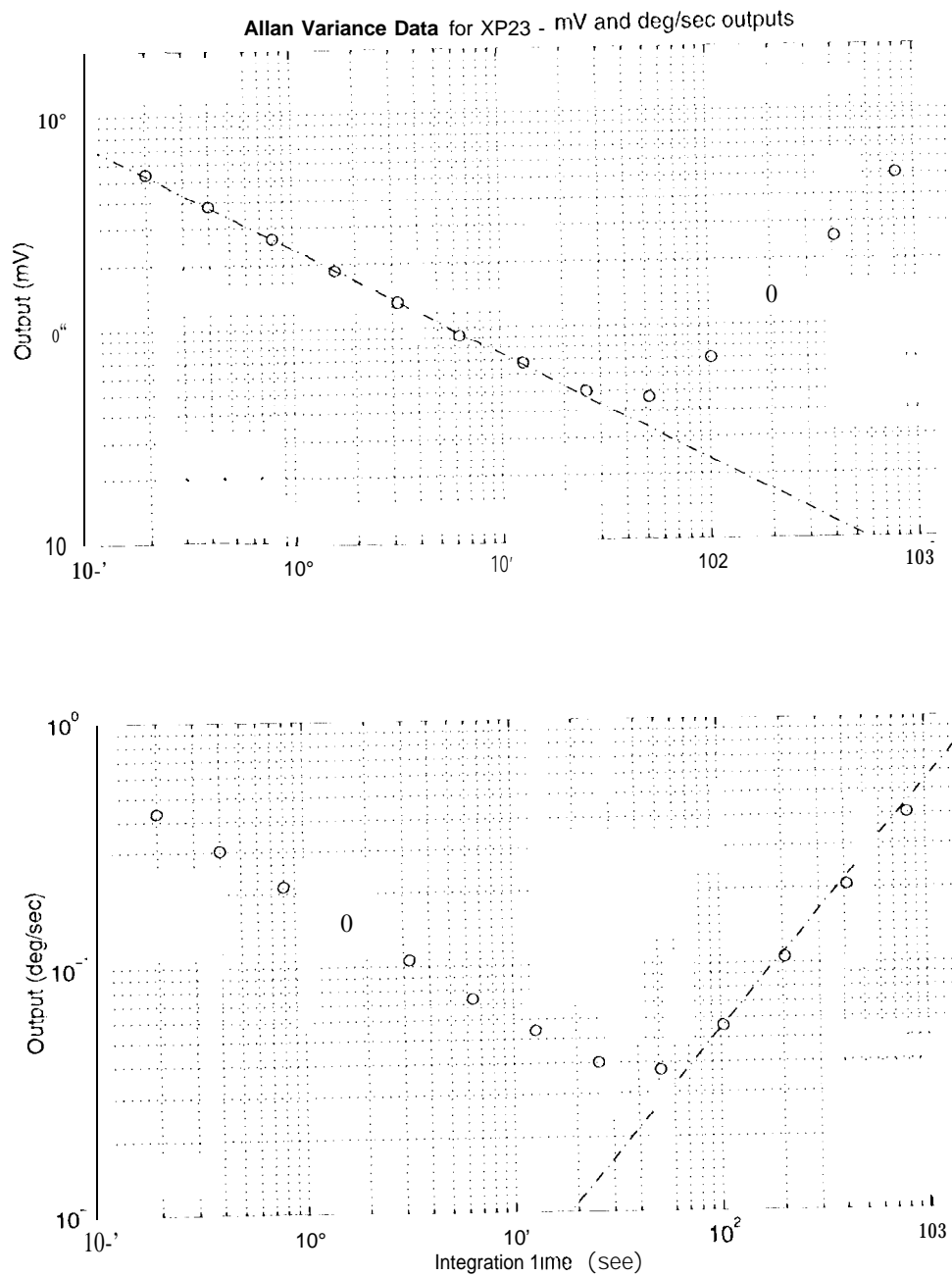
Figure 5-1: Allan Variance Data and Noise Asymptotes

Parameter	Center Value	Upper Limit	Lower Limit	Rate of Change
$K_\theta, K_\psi \left(\frac{NN\cdot m}{rad/sec}\right)$	1.58 x 10^{-4}			
$I_\theta, H_\psi \left(\frac{Kg}{m^2}\right)$	3.17 × 10^{-11}			
$\theta_{DC} \left(\frac{rad}{N\cdot m}\frac{rad}{N\cdot m}\right)$	**6326.6**			
$\psi_{DC} \left(\frac{rad}{N\cdot m}\right)$	**6326.6**			
$\omega_{\theta n}(t) \left(\frac{rad}{sec}\right)$	2759.4	2772	2747	3.14
$\omega_{\psi n}(t) \left(\frac{rad}{sec}\right)$	**2793.3**	2806	2780	3.14
$Q(t)$	75	100	50	
$K_{in} \left(\frac{N\cdot m}{V^2}\right)$	3.98 x 10$^{-\omega}$			
$K_{out} \left(\frac{m/s}{V}\right)$	3186			
$\Omega_q(t) \left(\frac{deg}{sec}\right)$	0			$(10.34 \times 10^{-4})\, t$
$\Omega_d(t) \left(\frac{deg}{sec}\right)$	0			$(10.34 \times 10^{-4})\, t$
$noise(t)$ (mV)	0	$(0.02754)\,\tau$	$(-0.02754)\,\tau$	random

Table 5.3: Summary of Calculated Values and Expected Ranges for X 1'-23

5.2 Simulation Techniques

5.2.1 Differential Equations

The final ordinary differential equations 4.15, 4.1 G, and 4.17 were simulated using a fourth order Runga Kutta algorithm. The actual sorce code is given in Appendix A. By writing a C program, is was possible to develop a simulation that was versitile, ran quickly, and could be ported to any system running a C compiler. Modular programming techniques will make the need to upgrade noise algorithms in the future fairly easy. It may also be possible to develop a Visual Basic front end and link this simulation to actual test data from a protoype gyroscope, so that the parameters calculated above can automatically be entered into the computer model.

5.2.2 Time Varying Parameters and Noise

The parameters are varied in very simple patterns which parallel quantitatively observed behavior. For a typical 50 second simulation, the resonance amplification

begins at some value and either remains fixed or is allowed to just steadily decay at a fixed rate, as if there were a pressure leak. This inital Q and ΔQ should be set more specifically once the acutal operating conditions are known. The resonant frequencies vary sinusoidally about their measured center frequencies.

The cross-coupled torque begins at a resonable value and then increases at the rate given in table 5.3 for the entire 50 seconds of the simulation. This reproduces the observed 1'(>s])011s(; of])rototype gyros(x)])('s. However, in the future, it may be neccesary to develop more sophisticated stochiastic models of gyro drift for longer simulations. Right now, the data to do this is unavailible.

The angle measurement noise is a random number within the bounds given in table 5.3. For simplicity, it is added to t he out put at the final recording stage.

5.2.3 Calculation of Amplitude and Phase

The amplitude needs to be calculated for both the output of the summing amplifier ($\dot{\theta}$) and the difference amplifier ($\dot{\psi}$). The program has a variable for the maximum and minimum value of each signal. If at any time, the present value of the signal is greater/less than the recorded maximum/minimum, this becomes the new maximum/minimum. Otherwise, the recorded value decays exponentially to zero. It will be necessary when using this simulation for performance predictions to run the output through a filter with the same characteristics as the one inherent to the lock-in analyzer, since these equations do not exist in the simulation, but do exist in the real circuit. It is much easier to generate the raw data and then use standard software programs to filter it, than to try and implement the circuit differential equations.

The zero crossing of each signal is also kept track of. The difference in the time for a zero crossing of $\dot{\theta}$ vs. $\dot{\psi}$ over the current period is the phase. This algorithm assumes no noise in its signals, which is true for this simulation. However, it should be exchanged in the future for a more robust process.

5.3 Simulation Verification
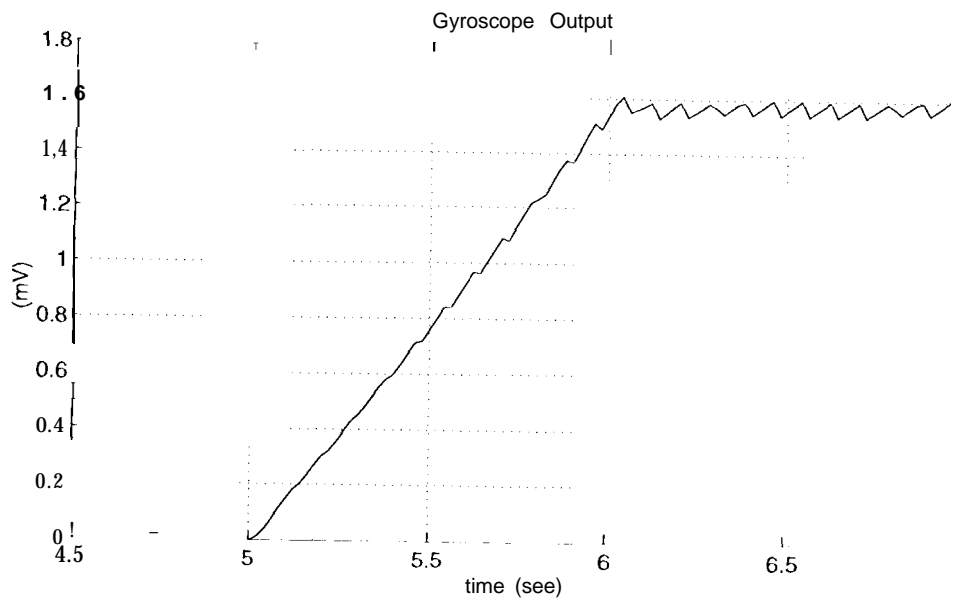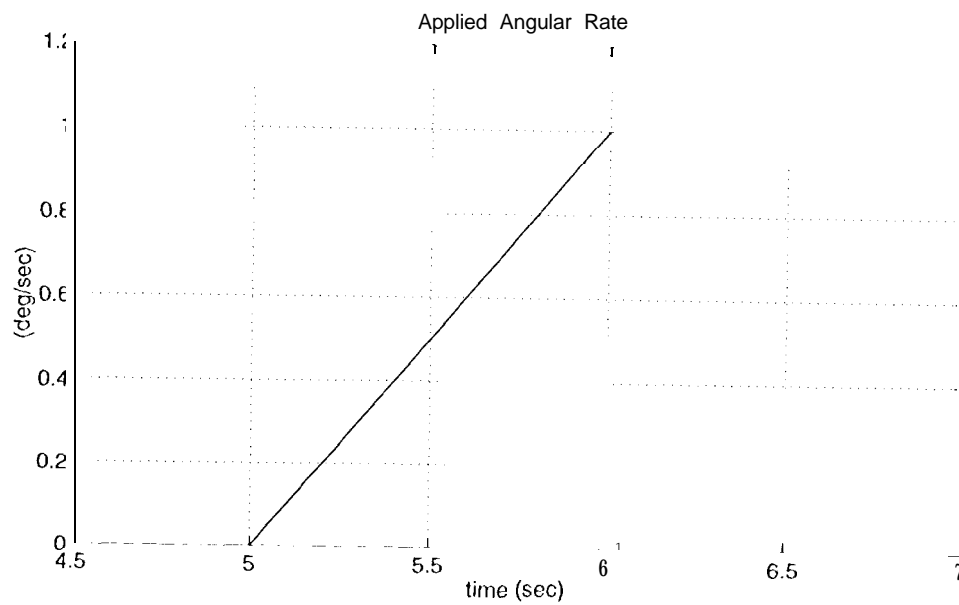
Figure 5-'2: Results from Simulation of Testing Conditions

45

The simulation was run with the testing operation conditions to see if the generated results corresponded to the experimental data. The parameters were the same as those calculated above. The Q of the system was allowed to remain constant at 75. Thermal noise and mechanical cross-coupling were set to O. Instead of the oscillator input, the gyro was driven by a 4 Vpp sinusoid at the sense resonant frequency. It was desired that a change in the applied angular rate of 1 $\frac{deg}{sec}$ would change the output by 1.25mV. The actual change, shown in figure 5-2, was 1.5 mV. As stated in a previous section the discrepency may be due to not knowing the exact amplification factor or the exact resonant frequency during the test, Or due to errors in the Runge-Kutta numerical method itself.

Chapter 6

Suggestions for Improvement

## 6.1 Machining and Assembly Improvements

Most of the imbalance errors and time varying effects experienced by this gyroscope design seem to be tracable to the fact that a brass post is glued to the micromachined silicon driving and sensing structure. The post itself can only by machined to tolerances achievable by a lathe, and even if these tolerances are good, the glue used in assembly will never be "balanced". One way to circumvent these drawbacks is to create a gyro that is entirely micromachined out of silicon. The structure will be more accurate, there will be few hand assembly steps, and the problem of non-uniform thermal expansion would disappear.

The challenge is to create high mass and high rotational inertia structures using micromachining techniques. Currently, it is impractical to etch a 5 mm vertical post integral to the cloverleaf paddle structure. Therefore, in an all-silicon structure, the "post" will have to be much smaller, perhaps on the order of 1 mm. I_θ and I_ψ are consequently orders of magnitude smaller, lowering the responsivity and increasing the resonant frequencies. Therefore, a twofold problem has been created for the sense electronics.

Another option is to look into alternate machining and assembly methods for the post. The post could be made by electroplating instead of lathing, resulting in a much better diameter tolerances. Also, a micromanipulator could be used in place

Original Configuration   Split Pad Configuration
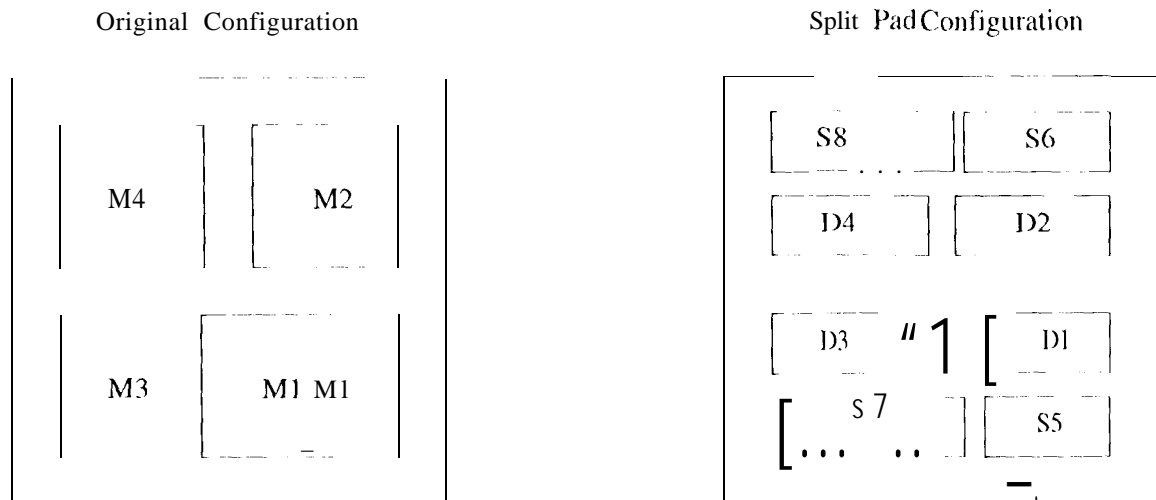
Figure 6-1: 1 Baseplate Electrode Split Configuration

of a person to insert the post, assuring that it is perfectly vertical with repect to the paddles. Finally, alternate glues should be investigated, since torr-seal, the current standard, has a tendency to aggregate during application.

6.2 Rebalanced Drive Actuators

The present driving scheme can only apply an attractive force on one side of the sense axis. It is possible, using several more strategically placed actuators and sensors, to observe and control the drive path completely. Using the quadrature error as feedback, a torque rebalance loop could be built around the gyro, which would at least align the principle axis of the vibration to the θ and ψ axis.

One simple way to accomplish this is to split the electrodes in the baseplate as shown in figure 6-1. Pads D1, D2, D3, and D4 are all drive while pads S5, S6, S7, and S8 are used for sensing. The sensing pads are further away from the origin of the instrument frame so that t hey would experience great er displacements and consequently have a higher reponsivity. Aonther possibility is to use a quartz "top plate" with four electrodes, identical to the baseplate. The gyro would be sandwiched between them, giving once again a total of eight pads to work with. The pads on

the top plate could be used for driving, and the baseplate for sensing, since the gyro element is identically grounded to both the drive and sense circuits.

6.3 Phase Sensitive Lock-in Analyzer

Currently, the lock-in analyzer circuit design is not phase sensitive. It only picks out the magnitude of the surpressed carrier frequency signal from the sense differential amplifier. As seen from the theory, this allows a large quadrature cross-coupled torque to be included into the output signal. If the lock-in design were phase sensitive, this zero signal could easily be removed. Figure 6-2 show the output of the simulation without phase sensitivity, where in quadrature cross-coupled torque is 9 times that of the in phase torque. This output is shown again in figure 6-3, but this time phase corrected with respect to $\dot{\theta}$. The improvement is both qualitatively and quantitatively obvious.

6.4 Separation of Drive and Sense Resonances

The final drifts discussed in chapter 4 where the resonant frequency drifts, phase drift and damping drift. Most of these problems would resolved by the self oscillating drive circuit, which servoes to a particular velocity for the drive. $\dot{\theta}$ is also used as the reference for the sense lock in, theoretically eliminating any harm done by frequency or damping drifts. The only problem arises when the sense resonance is close to the driving resonance. Then it is no longer guaranteed that the coriolis signal is in phase with the drive velocity. The only way to avoid this is to keep $\omega_{\psi n}$ a comfortable margin higher than $\omega_{\theta n}$, so that their resonant peaks never overlap, despite resonant frequency drifts, and no phase shift or variable amplification ever appears in the sense.

49

Applied Angular Rate

(deg/sec)

time (see)

Gyroscope Simulation Output

(mV)

time (see)
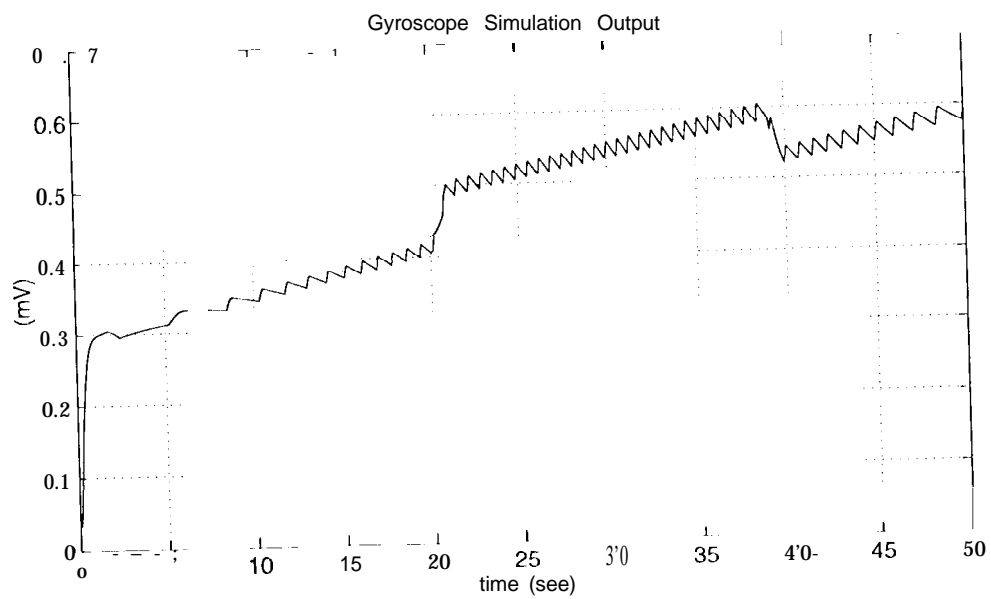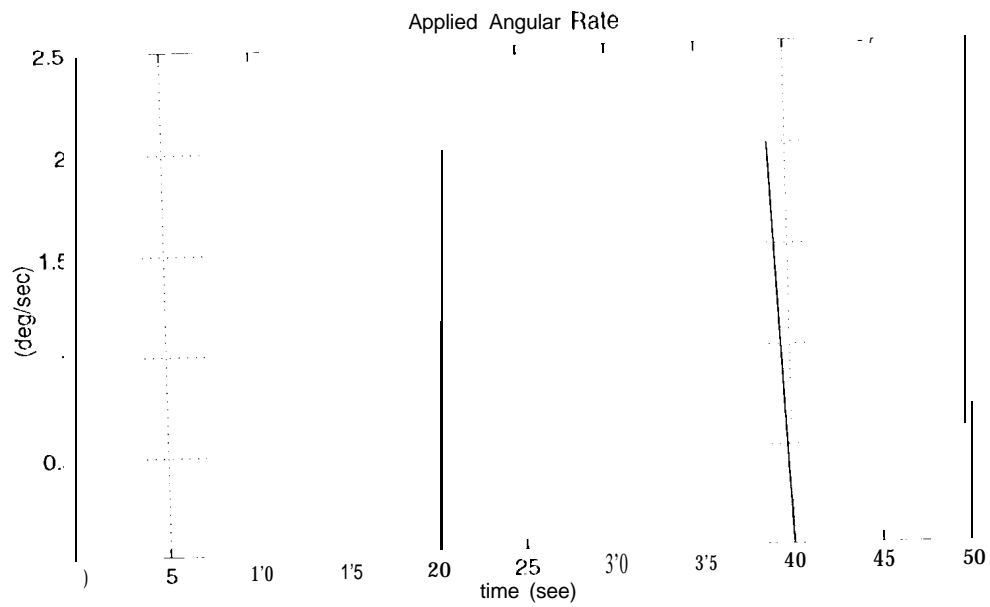
Figure 6-2: Simulation Output, no Phase Sensitivity

50
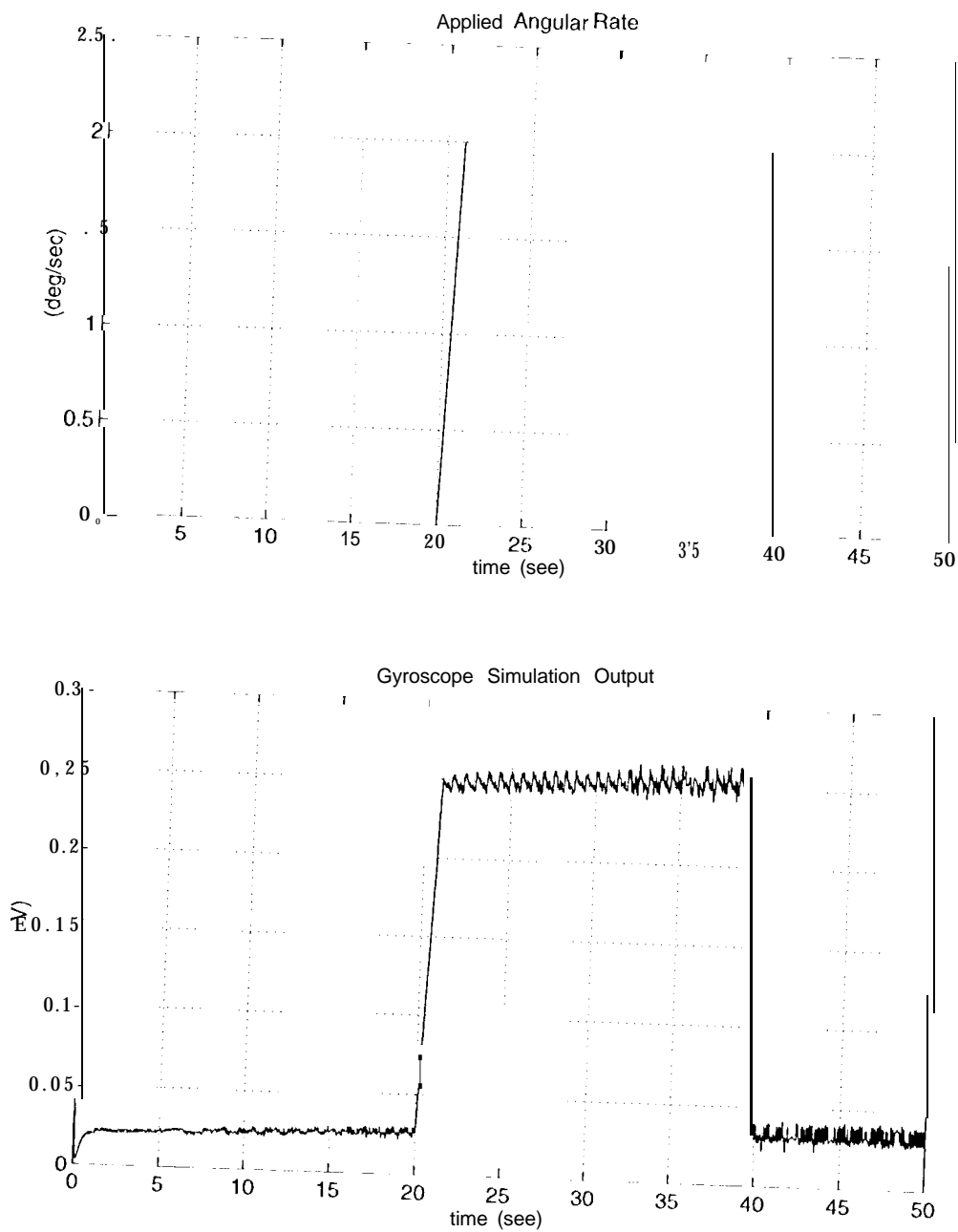
Figure 6-3: Simulation Output, Phase Sensitive

6.5 **Computer Control**

The gyroscope electronics designed to date have all been analog. If a small microchip capable of mathematical interpolations is added to the system, even higher performances could be achieved. For example, temperature could be compensated for by applying a temperature correction algorithm to the output. Also, if the CPU could recieve acceleration information from an outside source, the effects of non-uniform loading due to acceleration could be reduced. Finally, it would be possible to perform adaptive drive control to further refine the drive path, and "adaptive" sense control to change the integration time for minimum noise as needed.

Chapter 7

Conclusion

The theoretical equations presented at the end of chapter 2 are perfectly correct and useful for as far as they go. At the present stage of development of the JPL/UCLA microgyroscope project, it was necessary to create the next model which could simulate some important error character istics that the ideal equations could not reproduce. This purpose Of this paper was to determine the simplest way to reach that goal.

1 t was therefore necessary to develop some plausible theoretical basis for these new bahaviors and incorporate them into existing equations. The idea of time varying cross coupled torques fit the task perfectly. A s stated previously, there are many other sources of zero signal. J lowever, t he model for cress coupled torque satisfied the all the requirements of conforming to experiment al behavior while keeping the simulation efficient.

'] ']lis is still a work in progress. As the characterization process of the gyroscope improves, understanding of the sources and natures of t he errors will also become more refined. While this will obviously lead to better m odels, the end goals is a better understanding of the gyroscopes, and eventually, better gyroscopes.

Appendix A

Simulation Source Code

‑ ‑

```
#  include <math.h>
#  include <stdio.h>
#  include <stdlib.h>
#  include <math.h>
#  define NR_END 1
#  define FREE_ARG char*
#  define pi  3.141592654
#  define thetaDC 3687.6
#  define phiDC 3687.6
#  define Kout 1.593
```

10

```
float **y, *xx, *u;
float **w, **o, **c;
float output, out_max, out_min, out_amp, out_err, out_sign, out_ifb;
float  fb, fb_max, fb_min, fb_amp, fb_err, fb_pfb, fb_ifb;
float fb_zx0, fb_zx, fb_period, fb_out_phase;
float w_the, w_chi;
float q_the;
float  omega_y, omega_z;
float distq, distd, noise;
```

20

```
int out_q, fb_q;

float *vector(long nh) {float *V; v = (float *)malloc((size_t)((nh+1)*sizeof(float))); return v;}
```

```c
float **matrix (long int nr, long int nc) {

        long i;

        float **m;

        m = (float **) malloc((size_t)((nr+NR_END)*sizeof(float*)));

        if (!m) printf("allocation failure 1 in matrix o");

        m += NR_END;                                                          30

        m -= 1;

        m[1]=(float *) malloc((size_t)((nr*nc+NR_END)*sizeof(float)));

        if (!m) printf("allocation failure 2 in matrix;

        m[1] += NR_END;

        m[1] -= 1;

        for (i = 2; i <= nr; i++) { m[i] = m[i-1] + nc; } return m; }


void free_vector (float *v) {free ((FREE_ARG) (v));}
void free_matrix (float **v) { free ((FREE_ARG) v[1]); free ((FREE_ARG) (v));}

                                                                              40

void rk4 (float y[], float dydx[], float udat[], int n, [101 IMCX, double h, float yout[],
                          void (*derivs) (double, float[], float[], float[]))

{
        int i;
        float xh, hh, h6, *dym, *dyt, *yt;


        /* Allocate vectors */
        dym = (float *)malloc((size_t)((n+1)*sizeof( float)));
        dyt = (float *)malloc((size_t)((n+1)*sizeof(float)));
        yt = (float *)malloc((size_t)((n+1)*sizeof(float)));           50
        hh = h/2.0;
        h6 = h/6.0;
        xh = x + h}1;
        for (i = 1; i <= n; i++) {
                yt[i] = y[i] + hh*dydx[i];  }
        (*derivs) (xh, yt, dyt, udat);
        for (i= 1; i <= n; i++) {
                yt[i] = y[i] + hh*dyt[i];  }
        (*derivs) (xh, yt, dym, udat);
```

```
        for  (i = 1; i <== n; i++)

        {
                yt[i]  =  y[i] + h*dym[i];
                dym[i]  += dyt[i];

        }
        (*derivs) (x+h, y, dyt, udat);
        for (i =  1; i <= n; i++) {
                yout[i] = y[i] + h6*(dydx[i]  +  dyt[i] - 1 2.0*dym[i]); }
        /* Deallocate vectors */
        free ((FREE_ARG) (yt));
        free ((FREE_ARG) (dyt));
        free (( FREE_ARG) (dym));

}



void   store_data (int k)

{
        w[1][k]  =  w_the;
        w [2] [k] = w_chi;
        w[3][k]  =  q_the;
        o[1] [k] = omega_y;
        0[2] [k] = omega_z;
        0[3] [k] = out_amp + noise;
     o[4][k] = output;
        o[5] [k] = fb;
        c[1][k]  = fb_amp;
        c[2][k]  = fb_ifb;
        c[3] [k] .— fb_out_phase;
        c[4][k]  = distq;
        c[5][k]  =  distd;
        c[6] [k] = noise;



void   err_calc (double  t, double h,  int k, float  tau)

{
```

```
if (o[5][k] > fb_max) { fb_max = o[5][k]; }
else { fb_max = fb_max * (x]) (- n / w);  }


if (o[5][k] < fb_min) { fb_min = o[5][k]; }                              100
else { fb_min = fb_min * exp(-h/tau); }


fb_amp = fb_max - fb_min;
fb_err = fb_amp -- (2*pi*439.0*5 .0e-4*Kout);
fb_pfb = 1 #0 * fb_err;
fb_ifb = fb_ifb + 0.01 *fb_err*h;
    if (fb_ifb > 2000.0) fb_ifb = 2000.();
    if (fb_ifb < - 2000.0) fb_ifb = - 2000.0;


    switch (fb_q) {                                                      110
            case! (1) :        if (o[5][k] <= (0.5* fb_amp + fb_min)) {
                                              fb_zx0 = fb_zx;
                                              fb_zx =- t;
                                              fb_period =- 2*(fb_zx - fb_zx0);
                                              fb_q = · 1;}
                        break;
            case (-1):         if (o[5][k] >= (0.5 *fb_amp + fb_min)) {
                                              fb_zx0 = fb_zx;
                                              fb_zx = t;
                                              fb_period = 2* (fb_zx - fb_zx0); 120
                                              fb_q =-1 ; }
            default :           break; }


if (o[4] [k] > out_max)out_max = o[4] [k];
else out_max = out_max * exp(- h/tau);


if (o[4][k] < out_min) out_min = o[4][k];
else out_min = out_min * exp(-h/tau);

                                                                         130

out_amp = out_max -- out_min;
```

```
switch  (out_q) {

        case (1) : if (o[4][k] <=- ((0.5 *out_amp) + out_min)) {

                        fb_out_phase = (t  -  fb_zx)/fb_period;

                        out_q = - 1;}

                break;

        case  (-1):  if  (o[4][k] >= ((0.5 *out_amp) + out_min)) {

                        fb_out_phase : (t  -  fb_zx)/fb_period;

                        out_q = 1 ; }                                            140

        default  :  break; }


}


/******************************************************************************/


void  dist_calc(double t)

{
        q_the = 100.0() - 0.5*t;                                                150

        distq = w'_t,llc*O.9*10.34c- 4*(t +50);/ * y[1]driveamplitude */

        distd =      0.1*10.34(!-- 4*(t + 50); / * y[2], fb - drive velocity */

        w_the = 2 * pi * (400.0 + sin(2*pi*t/120.0));

        w_chi =- 2 * pi * (450.0 - sin(2*pi*t/240.0));
/*      noise = ((rand()/ 16. 385.0) - 1) * 0.000027 * sqrt(samps); */
/ '      if (t < 5.0) omega_z= 0.0;
        else if (t < 6.0) omega_z = 1.0*(pi/180.0)*(t- 5.0);
        else if (t < 9.0) omega_z = 1.0*(pi/180.0);
        else if (t < 10.0) omega_z = 1. 0*(pi/180.0) + 2.0*(pi/180.0) *(t- 9.0);
        else if (t < 14.0) omega_z = 3.0* (pi/180.0);                           160
        else if (t < 16.0) omega_z = 1.5*(pi/180. 0) *(16. 0- t);
        else omega_z= 0.0;
*/
        if (t  < 20.0) omega_z = 0.0;
        else if (t < 21.0)  omega_z = (2*pi/180)*(t - 20.0());
        else if (t < 39.0)  omega_z = (2*p i/180);
        else if (t < 40.0) omega_z = (2*pi/180)*(40-- t);
```

```
        else omega_z =  0.0;
```

```
}


/*************************************************************************/


void derivs (c1om1j1c t, float y[], float ydot[], float uder[])
{

        float w] 2, w22;
```

```
        w] 2 = w_the*w the;
        w22  = w_chi*w_chi;


/*      uder[1] = 2. 0*sin(2 *3. 141592654 *444.0*t) -t 2. 0; */
        uder[1] = - 100.0* fb_ifb*(fb/fb_amp);
        if (uder[1] > 5.0) uder[1] = 5.0;
        if (uder[1] < 0.0) uder[1 ] = 0.0;
        ydot[1 ] = y[2];
        ydot[2] = - (w1 2*y[1 ])- (w_the/q the*y[2])
                + thetaDC*w12*(3.9825e-10*(uder[1]+5)*(uder[1]+5));
        ydot[3] = y[4];
```

```
        ydot[4] = -- (( w22)*y[3])-((w_chi/q_the)*y[4])
                +phiDC*w2 2* 2*3.17e-11*((omega_z *y[2] )+(distq*y[1])+(distd*y[2]));


}




float  output_calc (float y[])
{
        return (Kout * y[4]);
}
```

```
float  fb_calc (float y[])
```

```c
{
    return (Kout * y[2]);

}


/**************************************************************************/
```

```c
int main ()
{
    float        1(X01(1 =- 3.50;
    float        end     =- 57.5001;
    float        pres    =   50.0;
    int          steps   =   2000;
    int          recpres =   2000;
    int          samps   =-  50;


/**************************************************************************/
```

```c
    int          order =  4 ;
    float        RC =  0.025;
    float        *vinit, *vlast;
    float        ulast;
    int          divs, divs2;
    int          i, j;
    int          k;
    int          counter =  0;
    double       x,h,x1,x2;
    float        *v, *vout, *dv, *uin;
    FILE         *fidx, *fidy, *fidu, *fidwq, *fidom, *fiderr;
```

```c

/** Allocating data vectors **/
    vlast = vector(order);
    vinit =- vector(order);
    xx    =- vector(steps + 1);
    w     =- matrix(3, steps +1);
```

```c
o = matrix(5, steps - 1);
e = matrix(6, steps + 1);
u = vector(steps + 1 ) ;
y = matrix(order, steps + 1 );
V = vector(order) ;
vout = vector (order + 1) ;
dv = vector (order + 1) ;
uin = vector (order);
```

```c
/** Initial Physical Values not in dist_calc **/
        w_the = 2 * 3.141592654 * 400.0;
        w_chi = 2 * 3.141592654 * 450.0;
        q_the = 1 25.0;
        distq = distd = 0.0;
    noise = 0.0;
        out_max = out_min = out_amp = 0.0;
        fb_max = fb_min = fb_err = 0.0;
        fb_amp = 0.01;
        fb_ifb = 0.0;
        fb_zx = fb_zx0 = fb_out_phase = 0.0;
        fb_period = 1.0 / w_the;
        out_q = fb_q = 1 ;
        omega_y = 0.0;
        omega_z = 0.0;
```

```c
/** Initial File data **/
        fidx = fopen ("xdata. txt", "w");
        fidy = fopen ("ydata .txt", "w");
        fidu = fopen ("udata. txt", "w");
        fidwq = fopen ("wqdata. txt", "w");
        fidom = fopen ("omdata. txt", "w");
        fiderr = fopen ("errdata .txt", "w");
```

```c
/** Initial Boundary Conditions (Small disturbance to drive) **/
        for (i = 1; i <= order;i++ ) {
                vlast [i] = 0.0; }
```

61

```
        vlast[2] = 1 .0e-5;


/**  Begin Simulation  **/
        I   *   for (divs = 0; divs < = (pres *end)-1; divs++ ) { */
        for  (divs2 = O;  divs2 <= (1 0*end - 1); divs2++ ) {                        280
          printf ("% .2f \n", divs2/10.0);
          for (divs = 0;  divs <= (pres - 1); divs++ ) {
                  for (i = 1; i <= order; i++ ) {
                          vinit [i] = vlast [i];  }
                  x1 = (divs2 + divs/pres)/1 0.0;
                  x 2  = (divs2 + (divs +1)/pres)/10.0;
                  for (i = 1; i <= order; i++ )

                  {
                          v[i] = vinit[i];
                          y[i][1] = v[i];                                           290

                  }
                  11[1] = ulast;
                  store_data(1);
                  xx[1] = x1;
                  x = x1;
                  11 = (x2 - xl) / steps;
                  dist_calc(x);
                  derivs (x, v, dv, uin);
                  rk4 (v, dv, uin, order, x, h, vout, derivs);
                  output = out pllt.talc(v) ;                                       300
                  fb = f-b-cm(v);
                  x += h;
                  xx[2] = x;
                  for (i = 1;  i <= order; i++ ){
                          v[i] = vout[i];
                          y[i][2] = v[i];}
                  u[2] = uin[ 1];
                  store_data (2);
                  for (k = 2; k <= steps; k++ ) {
                          dist-talc (x);                                           310
                          err_calc (x, h, k, RC);
```

62

```
            derivs (x, v, dv, uin);

            rk4 (v, dv, uin, order, x, II, vout, derivs);

            output = output_calc (v);

            fb  =  ft).talc(v);

            x += h;

            xx[k+ 1] = x;

            for (i = 1;  i <= order; i-1 +) {

                        v[i] = vout [i];

                        y[i][k+ 1] = v[i]; }                            320

            u[k+ 1] = uin[1];

            store_data (k + I);  }

    for (i = 1;  i <= order; i-1 +) {

                vlast[i] = y[i] [steps]; }

    ulast = u[steps];


/** Print to files  **/


    if (x1 >= record) {

            /*  printf ("%.4f\n",x1);*/                            330

            counter = counter + 1 ;

                if (counter >= (pres*10.0 /samps)) {

                  for (j= 1; j <= (steps / recpres); j++)

                     {

                            fprintf (fidx, "%g\n", xx[recpres*j]);


                            for (i = 1; i <= order; i++) {fprintf (fidy, "%g\t",y[i][recpres*j]); }
                            fprintf (fidy, "\n");


                            fprintf (fidu, "%g\n", u[recpres*j]);                            340


                            for (i = 1; i <= 3; i++) {fprintf (fidwq, "%g\t",w[i][recpres*j]); }
                            fprintf (fidwq, "\n");


                            for (i = 1; i <= 5;i++) { fprintf (fidom, "%g\t",o[i][recpres*j]); }
                            fprintf (fidom, "\n");
```

```
                                    for  (i = 1; i <= 6; i++ ) {fprintf (fiderr, "%g\t", e[i][recpres*j]); }
                                    fprintf (fiderr, "\n");

                          }                                                                          350
                    counter = 0;}

          }

        }

      }


/**CLean up 'HKII1OIVJ**/
          free_vect or (uin);
          free_vector ((IV);
          free_vector (vout) ;
          free_vector (v) ;                                                                          360
          free_matrix (y);
          free_vector (11);
          free:.lllatrix  (c);
          free_matrix (o);
          free_matrix (w);
          free_vector  (xx);
          free_vector (vinit);
          free_vector (vlast) ;
          f('lose (fidx);
          fclose (fidy);                                                                             37(l
          fclose (fidu);
          fclose (fidwq) ;
          fclose (fidom);
          fclose (fiderr) ;
          printf ("\nDONE\n");
          return (0);


      }


                                                                                                    38(l
```

Bibliography

[1] Richard W. Bush. Research on Vibratory Gyroscopes. Technical report, MIT, Electronic Systems Laboratory, Department of Electrical Engineering, Cambridge, MA, June 1966.

[2] George W. Erickson. An Overview of Dynamic and Stochastic Modeling of Gyros. In *Proceedings of the 1993 National Technical Meeting of the Institute of Navigation*, pages 339 351, Alexandria, VA, 1993. Institute of Navigation.

[3] Charles T. Morrow. Zero Signals in the Sperry Tuning Fork Gyrotron. *The Journal of the Acoustical Society of America*, 27(3):581 585, May 1955.

[4] Vatche Vorperian and Christopher B. Stell. An All-Electrical Design-Oriented Model of a Micromachined Vibratory Gyroscope. Unpulblished notes, November 1995.

[5] Jaroslava Z. Wilcox. Cloverleaf Vibratory Gyroscope 1: The Dynamical Behavior and Device Design. Unpublished JPL Memo, November 1995.